

Current Biology

Conserved Biochemical Defenses Underpin Host Responses to Oomycete Infection in an Early-Divergent Land Plant Lineage

Highlights

- *Marchantia* liverworts display a dynamic molecular response to oomycete infection
- Features of conserved defenses are present in liverworts and angiosperms
- Distantly related plants activate phenylpropanoid metabolism during infection
- MpMyb14 regulates oomycete-induced biochemical defenses in liverworts

Authors

Philip Carella, Anna Gogleva,
David John Hoey,
Anthony John Bridgen,
Sara Christina Stolze,
Hirofumi Nakagami,
Sebastian Schornack

Correspondence

sebastian.schornack@slcu.cam.ac.uk

In Brief

Carella et al. investigate host-pathogen infection dynamics in the early-divergent model liverwort *Marchantia polymorpha* and the angiosperm *Nicotiana benthamiana*. Their results identify features of an evolutionarily conserved biochemical defense response in land plants that is mediated by an R2R3-MYB transcription factor in liverworts.



Conserved Biochemical Defenses Underpin Host Responses to Oomycete Infection in an Early-Divergent Land Plant Lineage

Philip Carella,¹ Anna Gogleva,¹ David John Hoey,¹ Anthony John Bridgen,¹ Sara Christina Stolze,² Hirofumi Nakagami,² and Sebastian Schornack^{1,3,4,*}

¹Sainsbury Laboratory, University of Cambridge, Bateman Street, Cambridge CB2 1LR, UK

²Protein Mass Spectrometry Group, Max Planck Institute for Plant Breeding Research, Carl-von-Linne-Weg, Cologne 50829, Germany

³Department of Plant Sciences, University of Cambridge, Downing Street, Cambridge CB2 EA3, UK

⁴Lead Contact

*Correspondence: sebastian.schornack@slcu.cam.ac.uk

<https://doi.org/10.1016/j.cub.2019.05.078>

SUMMARY

The expansion of plants onto land necessitated the evolution of robust defense strategies to protect against a wide array of microbial invaders. Whereas host responses to microbial colonization are extensively explored in evolutionarily young land plant lineages such as angiosperms, we know relatively little about plant-pathogen interactions in early-diverging land plants thought to better represent the ancestral state. Here, we define the transcriptional and proteomic response of the early-divergent liverwort *Marchantia polymorpha* to infection with the oomycete pathogen *Phytophthora palmivora*. We uncover a robust molecular response to oomycete colonization in *Marchantia* that consists of conserved land plant gene families. Direct macroevolutionary comparisons of host infection responses in *Marchantia* and the model angiosperm *Nicotiana benthamiana* further reveal a shared set of orthologous microbe-responsive genes that include members of the phenylpropanoid metabolic pathway. In addition, we identify a role for the *Marchantia* R2R3-MYB transcription factor MpMyb14 in activating phenylpropanoid (flavonoid) biosynthesis during oomycete infection. Mpmyb14 mutants infected with *P. palmivora* fail to activate phenylpropanoid biosynthesis gene expression and display enhanced disease susceptibility compared to wild-type plants. Conversely, the ectopic induction of MpMyb14 led to the accumulation of anthocyanin-like pigments and dramatically enhanced liverwort resistance to *P. palmivora* infection. Collectively, our results demonstrate that the *Marchantia* response to oomycete infection displays evolutionarily conserved features indicative of an ancestral pathogen deterrence strategy centered on phenylpropanoid-mediated biochemical defenses.

INTRODUCTION

Plants have engaged in close interactions with microbial life forms throughout their evolutionary history. Fossils obtained from the Rhynie chert demonstrate the presence of fungal hyphae and endosymbiotic structures within cells of >400 million-year-old seedless vascular land plants, which suggests that the colonization and expansion of plants on land may be tightly linked with the ability to accommodate microbes [1, 2]. Limited evidence also supports the idea that ancient land plants were attacked by pathogens, as oomycete-like organisms are present in fossilized plant detritus in the Rhynie chert [3, 4]. Moreover, the fossils of *Nothia aphylla* (Early Devonian, vascular) cells colonized by fungus-like organisms display signatures of cell-wall-associated responses that are typically directed to intruding filamentous microbes in extant plants [4, 5]. The green plant lineage has since evolved and diversified into the various families present today, from the early-diverging bryophytes (liverworts, mosses, hornworts) to the evolutionarily young flowering seed plants (angiosperms). Our current understanding of how plants respond to microbes is heavily centered on angiosperms and is described in great detail at the metabolic, transcriptional, and proteome levels. In general, angiosperms employ a tiered immune system mediated by pattern recognition receptors (PRRs) that recognize broadly conserved microbial MAMPs (microbe-associated molecular patterns) or by nucleotide-binding leucine-rich repeat (NLR) proteins that directly and/or indirectly monitor pathogen virulence factors [6–8]. In many cases, the activation of PRR- or NLR-mediated immunity in angiosperms leads to the conserved induction of defense hormones (salicylic acid, jasmonic acid), secretion of pathogenesis-related (PR) proteins, cell-wall reinforcement, and phenylpropanoid-associated biochemical defenses (polyphenols, flavonoids, anthocyanins, phytoalexins) [8–10]. By comparison, we know relatively little about how early-diverging land plant lineages respond to invading microbes, which limits our ability to identify core plant defense mechanisms representative of ancestral traits that likely contributed to the colonization and expansion of plants on land.

Bryophytes are non-vascular, gametophyte-dominant (haploid) land plants that are thought to have evolved key traits essential to life on land. Recent phylogenetic analyses suggest that the



bryophytes represent a monophyletic group of early-diverging land plants, wherein liverworts and mosses are united in the “Setaphyta” clade that is distinct from hornworts [11–13]. Evolutionarily conserved traits associated with metabolism, abiotic stress tolerance, and plant development are well described in bryophyte model systems such as the moss *Physcomitrella patens* or the liverwort *Marchantia polymorpha* [14, 15]; however, our understanding of their ability to sense and respond to microbes is only now being investigated in more detail [16–18]. Much of this effort has centered on interactions with beneficial symbiotic microbes, such as fungi belonging to the Glomeromycotina (arbuscular mycorrhizal fungi) or Mucoromycotina (Endogone fungi). These works have revealed the widespread conservation of plant genes essential for symbiosis across land plants and their algal predecessors [19] and have also uncovered the physiological and environmental benefits of dual and contrasting fungal associations that likely shaped plant life on land [20]. Bryophyte-pathogen interactions are comparatively less well resolved. In mosses, several pathosystems have been established between necrotrophic filamentous pathogens and the model moss *P. patens* [16]. Recent studies have also revealed the conservation of MAMP and PRR-mediated immune pathways involved in the perception of fungal chitin epitopes in mosses [21]. Interactions with biotrophic or hemi-biotrophic pathogens (*Colletotrichum*, *Phytophthora*) that manipulate living plant cells have been investigated in *Physcomitrella*; however, specialized intracellular microbial infection structures (such as haustoria) are not observed in these plants [22, 23].

The dioecious liverwort *M. polymorpha* has gained significant traction as an early-divergent bryophyte model system for comparative evolutionary analyses of molecular plant-microbe interactions. *M. polymorpha* and other bryophytes utilize a conserved “jasmonic acid” signaling module that functions through the jasmonic acid (JA) precursor dinor-OPDA (12-oxo-phytyldienoic acid) rather than JA itself, indicative of ligand-receptor co-evolution in the JA or OPDA pathway across plants [24]. This fits well with phylogenetic analyses of core plant immunity genes that appear to be conserved in the *M. polymorpha* genome [15]. An ecological survey of wild *M. polymorpha* liverworts identified several genera of endophytic fungi with beneficial or detrimental impacts on liverwort growth *in vitro*; however, a mechanistic understanding of these interactions remains to be clarified [25]. We recently established a robust pathosystem between the hemi-biotrophic oomycete pathogen *Phytophthora palmivora* and *M. polymorpha*. *P. palmivora* hyphae efficiently colonize the dorsal photosynthetic layer of several liverwort species and develop intracellular infection structures that invaginate living host cells (biotrophy) specifically in this tissue layer [26]. Similar to observations in angiosperms, cellular trafficking machinery (Rab GTPases and the membrane syntaxin MpSYP13B) was directed to intracellular infection structures in *Marchantia* [26], which suggests that phylogenetically distant land plants employ equivalent defense responses that may have been conserved throughout their evolutionary history. Ultimately, *P. palmivora* shifts to a necrotrophic lifestyle where plant tissues are actively destroyed to release additional nutrition.

In this study, we performed RNA sequencing (RNA-seq) and proteome analyses to reveal molecular responses occurring in *M. polymorpha* liverwort thalli during infection with

P. palmivora. This identified evolutionarily conserved loci responsive to pathogen infection that included small secreted PR proteins, transcription factors, and vesicular trafficking machinery among other gene families. To gain further evolutionary insight, we performed comparative RNA-seq analysis against a *Phytophthora* angiosperm (*Nicotiana benthamiana*) leaf infection time course, which facilitated the discovery of orthologous groups of pathogen-responsive *Marchantia* and *Nicotiana* genes associated with phenylpropanoid and flavonoid biosynthesis. Consistent with these data, we uncovered a role for a phylogenetically basal R2R3-MYB transcription factor, MpMyb14, in mediating flavonoid-associated biochemical defenses during pathogen infection in *M. polymorpha* thalli. Mpmyb14 mutants exhibited enhanced susceptibility to *P. palmivora* infection, whereas the ectopic over-accumulation of MpMyb14-regulated pigments dramatically suppressed pathogen growth *in planta*, suggesting a protective role for these compounds during biotic stress. Together, these data provide further support for the conservation of biochemical defenses in phylogenetically distant model plants.

RESULTS

Dynamic Alteration of the *M. polymorpha* Transcriptome and Proteome during Infection by *P. palmivora*

To understand how *M. polymorpha* responds to infection, we performed time-resolved RNA-seq analysis comparing the transcriptional profiles of 3-week-old TAK1 (male) liverworts spot inoculated with water (mock) or a suspension of *P. palmivora* ARI-tdTomato (ARI-td) zoospores. Differential expression analysis (\log_2 fold change [LFC] ≥ 2 and adjusted $p < 10^{-3}$) of mock versus infected thalli sampled daily from 1 to 4 days post inoculation (dpi) revealed that infected liverworts undergo a pronounced shift in their transcriptional profiles compared to mock-treated controls, which is observed at 1 dpi and is strongest at 4 dpi (Figures 1A and 1B; Data S1). The total number of differentially expressed genes gradually increased throughout the time-course experiment to a maximum of 439 downregulated and 968 upregulated genes at 4 dpi (Figure 1B), with many of these genes showing significant differential expression between 2 and 4 dpi (Figure 1C). To further support these data, we performed liquid chromatography-tandem mass spectrometry (LC-MS/MS)-based proteomics comparing *P. palmivora*-infected versus mock-treated TAK1 thalli at 4 and 8 dpi, which represent biotrophic and necrotrophic infection stages, respectively (Data S2). We identified 150 *M. polymorpha* proteins that were significantly enriched in *P. palmivora*-infected TAK1 thalli at both 4 and 8 dpi, with 93 proteins uniquely accumulating at 4 dpi during biotrophy and 262 proteins accumulating at 8 dpi during necrotrophy (Figure 1D; Data S2). A total of 137 proteins were consistently less abundant at both time points during infection, with only 76 proteins specifically depleted during biotrophy and 584 depleted proteins during the necrotrophic stage where plant tissues are actively destroyed by the pathogen (Figure 1D; Data S2). A comparison of the RNA-seq and proteomics datasets at 4 dpi (biotrophy) revealed 187 *M. polymorpha* loci that were consistently more abundant during infection and 36 loci that were consistently attenuated (Figure 1E). Together, these data reveal a dynamic molecular response in

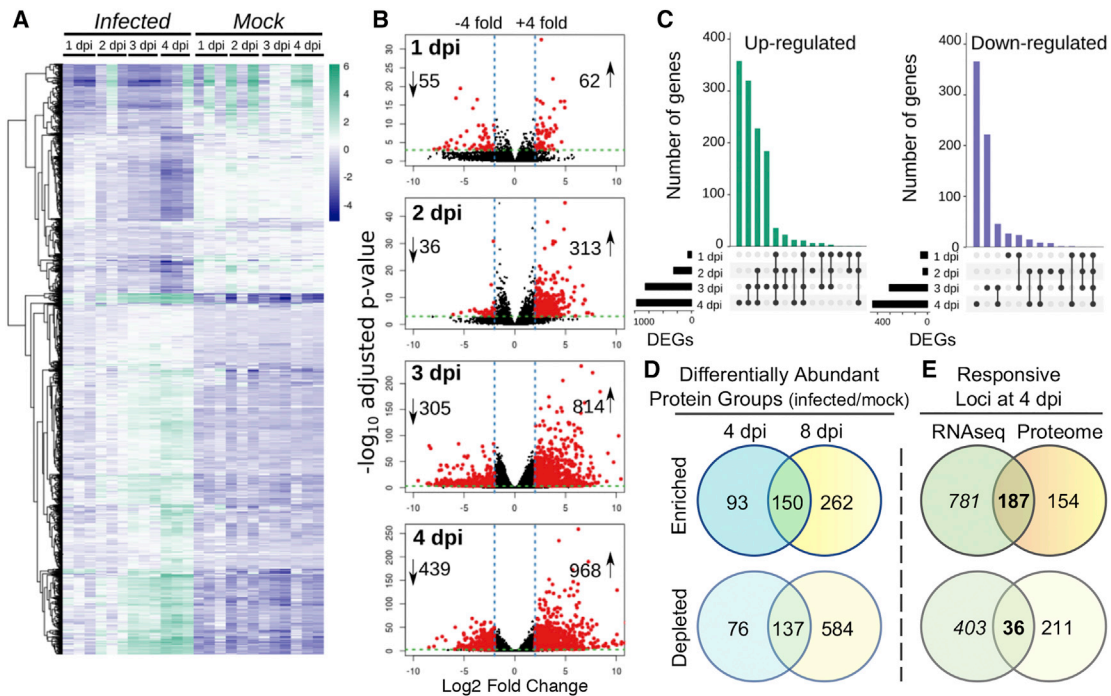


Figure 1. *M. polymorpha* Undergoes a Dynamic Transcriptional and Proteomic Response during Infection with *P. palmivora*

(A) Hierarchical clustering of significantly differentially expressed genes during *P. palmivora* infection (adjusted $p < 10^{-3}$; \log_2 fold change [$|\text{LFC}| \geq 2$]; variance-stabilized row-centered counts are shown. Time points represent days post inoculation (dpi).

(B) Volcano plots displaying pairwise differential expression analysis per time point of *P. palmivora*-infected versus mock-treated samples at the indicated time points. Significantly differentially expressed genes are displayed in red.

(C) UpSet plots showing shared and time-point-specific upregulated and downregulated *M. polymorpha* genes.

(D) Total numbers of differentially abundant (enriched or depleted) *M. polymorpha* protein groups in *P. palmivora*-infected versus mock-treated liverworts at 4 and 8 dpi.

(E) Comparison of differentially regulated *M. polymorpha* loci identified at 4 dpi in the RNA-seq and proteomics analyses.

See also [Data S1](#) and [S2](#).

M. polymorpha thalli that are colonized by the hemi-birotrophic oomycete *P. palmivora*.

Angiosperm PR Gene Families Are Similarly Induced during Infection in *Marchantia*

A hallmark of many plant-microbe interactions is the transcriptional induction of *PR* genes that typically encode small secreted proteins with predicted or demonstrated antimicrobial activity [27–29]. These families are generally conserved among seed plants and are expressed during various plant-microbe interactions [28, 30]. To assess whether *PR* genes are similarly utilized in *M. polymorpha*, we identified candidate *PR* gene families (based on pfam domains) and assessed whether these loci are significantly upregulated in the *Marchantia*-*P. palmivora* RNA-seq infection time course. A number of candidate *PR* genes representing well-characterized families were identified (Figure S1), which encode small cysteine-rich secreted proteins (*PR1*), several glucanases and chitinases (*PR2*, *PR3*, *PR8*, *PR11*), protease inhibitors (*PR6*), subtilases (*PR7*), peroxidases (*PR9*), lipid transfer proteins (*PR14*), and cupins (*PR15/16*). Next, we increased the stringency of this search by identifying *PR* gene members displaying significant protein accumulation in the *Marchantia*-*Phytophthora* interaction proteome. This revealed support for the accumulation of *PR1*, *PR2*, *PR3*, *PR5*, *PR6*,

PR9, and *PR15* family members during infection (Figure 2A; Data S2). Notably, members of the *PR6* (protease inhibitor) and *PR9* (peroxidase) gene families were among the most highly induced loci observed in the *Marchantia*-*Phytophthora* time-course datasets and included the previously characterized *MpPRX* (Mapoly0106s0049) locus [26]. To visualize the transcriptional induction of these loci *in planta*, we generated promoter-reporter lines in the TAK1 background and challenged thalli of these plants with *P. palmivora*. Transcriptional fusions of the *MpPR6a* (Mapoly0448s0001) and *MpPRX/PR9* promoters to nuclear-localized fluorescent reporters (tdTomato-NLS) demonstrated a strong induction of both genes during infection with yellow fluorescent protein (YFP)-labeled *P. palmivora* (isolate L1L1) at 3 dpi (Figure 2B). The transcriptional induction of *MpPR6a* and *MpPRX/PR9* was observed in cells that were in direct contact with *P. palmivora* hyphae as well as uncolonized neighboring cells (Figure 2B). Analysis of promoter:*GUS* lines demonstrated that a 1.8-kb fragment of the *MpPR6a* promoter was sufficient to drive *GUS* expression in *P. palmivora*-colonized air chambers along liverwort thalli compared to mock-treated controls (Figure 2C). This is in contrast to previously characterized *MpPRX/PR9*::*GUS* lines that demonstrated a strong induction of *GUS* activity throughout the thallus of infected liverworts [26]. Collectively, these data demonstrate that *PR* gene families

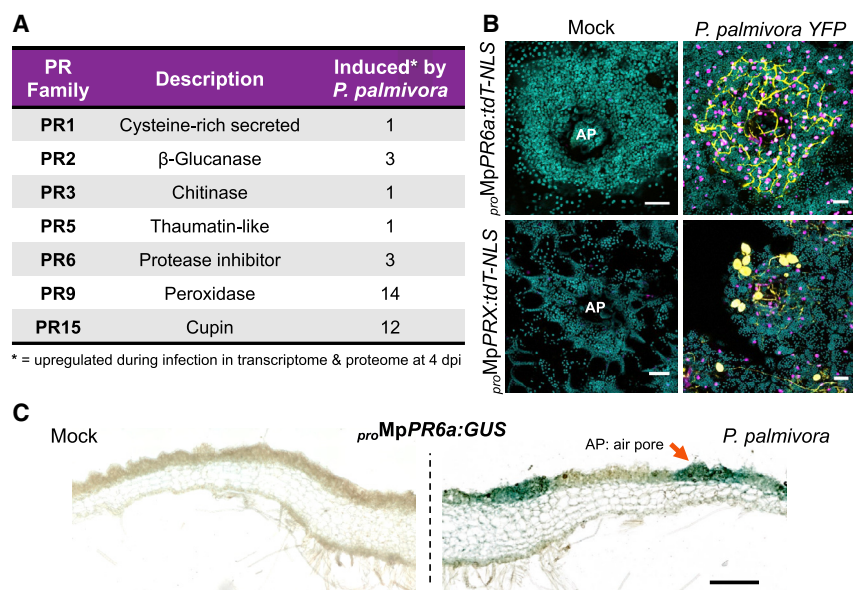


Figure 2. PR Protein Families Are Activated in Oomycete-Colonized *M. polymorpha* Thalli

(A) Identification and description of *M. polymorpha* PR gene families displaying transcript and protein accumulation during infection with *P. palmivora*. See also [Data S1](#) and [S2](#) and [Figure S1](#).

(B) Visualization of MpPR6a and MpPRX/PR9 promoter activation in air chambers of 3-week-old *proMpPR6a:tdTomato-NLS* and *proMpPRX/PR9:tdTomato-NLS* lines 3 dpi with *P. palmivora*-YFP (isolate LILI-KDEL-YFP) or mock-treated with water. Air pores (APs) are labeled at the center of the pore. Scale bars, 50 μ m.

(C) Tissue-level expression analysis of *proMpPR6a:GUS* liverworts infected with *P. palmivora* (ARI-td) or mock-treated with water. Cross-sectioned thalli were stained 7 dpi. An arrow indicates an AP on the dorsal liverwort surface. Scale bar, 0.5 mm. All images are representative of results collected from at least 6 independent treatment (mock or infected) sites.

are activated during the colonization of liverwort thalli by an oomycete pathogen in a manner similar to vascular plants, which suggests a conserved and perhaps ancestral role for PR gene families in plant-pathogen interactions across land plants.

Marchantia Responds to Pathogen Infection with a Diverse Set of Conserved Gene Families

To gain further insight into the classes of *M. polymorpha* loci responding to *P. palmivora* infection, we focused our analysis of the RNA-seq and proteomics datasets on the annotations and phylogenetic analyses of conserved land plant gene families described in [15]. This revealed a diverse set of *Marchantia* gene families responding to *P. palmivora* infection, including those associated with transcriptional regulation, the cell wall and cuticle, hormone biology, phenylpropanoid (flavonoid) biosynthesis, lipid peroxidation, terpene synthesis, vesicular trafficking, transporters and membrane H^+ -ATPases, kinases, and receptors (Figure 3A). Categorized heatmaps displaying the differential abundance of these loci during infection are displayed in [Data S3](#). Using qRT-PCR analysis, we validated a subset of pathogen-responsive *Marchantia* loci, which showed significant increases in transcript abundance in TAK1 thalli infected with *P. palmivora* compared to mock-treated controls (Figure S2A). The RNA-seq analysis also confirmed the pathogen-induced upregulation of the membrane-localized syntaxin MpSYP13B and dirigent-like MpDIR genes that were previously demonstrated to be transcriptionally induced during infection with *P. palmivora* [26]. Together, these data demonstrate the differential accumulation of broadly conserved plant gene families during pathogen infection in *M. polymorpha* thalli.

A Set of Shared Orthologous Genes Responds to Oomycete Colonization in *M. polymorpha* and the Angiosperm *N. benthamiana*

Our expression studies in *Marchantia* suggested that liverworts activate conserved land plant gene families during infection with *P. palmivora*. However, the extent to which liverworts and

angiosperms regulate the same groups of conserved orthologous genes during oomycete colonization was unknown. To address this, we performed infection time-course RNA-seq in the model angiosperm *N. benthamiana* for comparison against the *Marchantia-Phytophthora* transcriptome. Leaves of 3-week-old *N. benthamiana* plants were inoculated with *P. palmivora* ARI-td zoospores or water (mock treatment) and analyzed at 14, 24, 48, and 72 h post inoculation (hpi) because these time points encompass comparable *P. palmivora* infection stages (early to late biotrophy and sporulation) [26, 31]. RNA-seq analysis comparing mock-treated and *P. palmivora*-infected *N. benthamiana* leaves similarly revealed a prominent shift in transcriptional profiles during infection, with a steady increase in the total number of differentially regulated genes at later stages of infection (Figure S2B). To compare the *Marchantia* and *Nicotiana* infection-expression profiles, we first identified groups of orthologous protein-coding genes (orthogroups) using OrthoFinder [32]. This revealed a total of 7,156 orthogroups shared between *M. polymorpha* and *N. benthamiana*, of which 2,494 were single-copy orthologs likely representing genes with evolutionarily conserved functions. Because a large divergence time separates the evolution of liverworts and angiosperms, we assessed similarity in host responses to *Phytophthora* infection by focusing on the differential expression of single-copy orthologs shared in *M. polymorpha* and *N. benthamiana*. On average, ~80% of differentially expressed orthologs responded in the same direction across time points (i.e., up- or downregulated during infection in liverworts and angiosperms), whereas ~20% of loci responded in opposing directions (Figure 3B; [Data S1](#)). Several of these responsive single-copy orthogroups belonged to conserved gene families, which included PR proteins, signaling machinery (mitogen-activated protein kinases [MAPKs], receptor-like kinases [RLKs], transcription factors), transporters, trafficking machinery, and cell-wall-related proteins (Figure 3B). Genes classically associated with phenylpropanoid and flavonoid biosynthesis were among the most consistently/similarly responsive groups

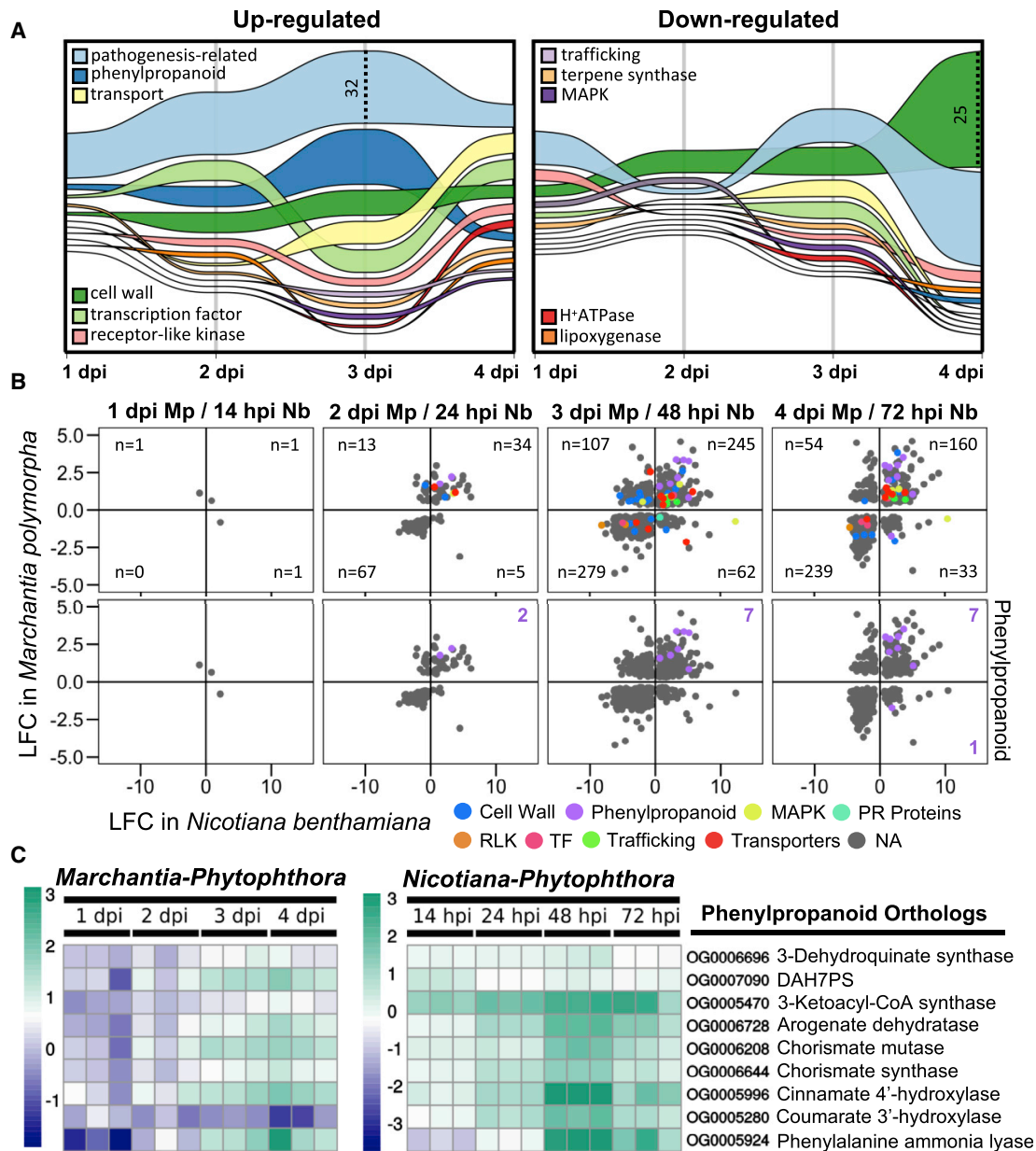


Figure 3. Oomycete-Colonized *M. polymorpha* Liverworts Exhibit Features of an Evolutionarily Conserved Transcriptional Response to Pathogen Infection

(A) Alluvial diagrams summarizing overall transcriptional dynamics of *M. polymorpha* gene families that are differentially expressed during infection. Relative width of the alluvial band corresponds to the number of differentially expressed genes at a given time point (MAPK, mitogen-activated protein kinase; PR, pathogenesis-related; TF, transcription factor; RLK, receptor-like kinase).

(B) Similarity of transcriptional responses of single-copy orthologous genes in *P. palmivora* (ARI-td)-infected *M. polymorpha* thalli and *N. benthamiana* leaves. Scatterplots display the direction (LFC) of transcriptional changes of single-copy orthologs during infection in both hosts. Significantly differentially expressed single-copy orthologs with adjusted $p < 10^{-3}$ are shown.

(C) Differential expression of single-copy phenylpropanoid-pathway-related genes in *M. polymorpha* and *N. benthamiana* during oomycete infection. Variance-stabilized row-centered counts are shown for *P. palmivora*-infected plant samples. See also Data S1 and S3 and Figure S2.

of conserved orthologous gene families activated during the colonization of liverwort and angiosperm host tissues by *P. palmivora* hyphae, with the exception of a single *C3'H* (coumarate 3'-hydroxylase) gene that was downregulated in *Marchantia*

and upregulated in *Nicotiana* (Figures 3B and 3C). Collectively, these data reveal similarity in *Marchantia* and *Nicotiana* responses to pathogen infection despite the large phylogenetic distance separating liverworts and angiosperms.

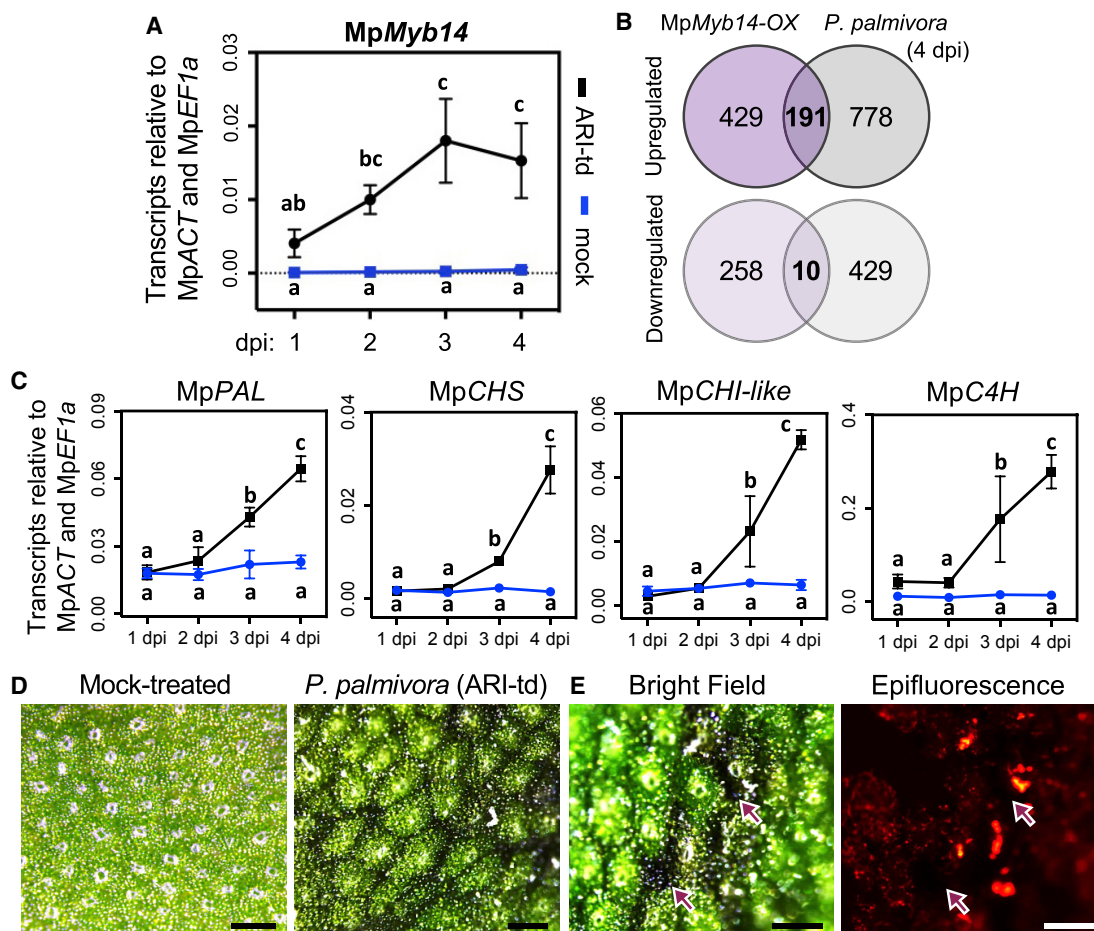


Figure 4. MpMyb14 Upregulation Coincides with the Induction of Flavonoid Biosynthesis Genes and Pigment Accumulation in *P. palmivora*-Colonized *Marchantia* Thalli

(A) qRT-PCR analysis of *MpMyb14* transcripts in mock-treated or *P. palmivora*-colonized (ARI-td) TAK1 plants ($n = 8$ per time point and treatment) from 1 to 4 dpi. Expression values are shown relative to internal *MpACT* and *MpEF1a* controls. Different letters signify statistically significant differences in transcript abundance (ANOVA, Tukey's honestly significant difference [HSD], $p < 0.05$). Error bars represent SD.

(B) Overlap between transcriptional profiles of *MpMyb14*-overexpressing (OX) liverworts [37] compared to *P. palmivora*-infected TAK1 thalli at 4 dpi. See also Data S1.

(C) qRT-PCR analysis of phenylpropanoid and flavonoid pathway genes (*MpPAL*, phenylalanine ammonia lyase Mapoly0005s0089; *MpCHS*, chalcone synthase Mapoly0021s0159; *MpCHI-like*, chalcone-flavone isomerase-like Mapoly0175s0004; *MpC4H*, cinnamate-4-hydroxylase Mapoly0163s0018) in mock-treated or *P. palmivora*-colonized (ARI-td) TAK1 plants from 1 to 4 dpi. Expression values are shown relative to internal *MpACT* and *MpEF1a* controls. Different letters signify statistically significant differences in transcript abundance (ANOVA, Tukey's HSD, $p < 0.05$). Error bars represent SD.

(D) Bright-field micrographs of mock-treated (water) and *P. palmivora*-infected TAK1 thalli (5 dpi) illustrating pathogen-dependent accumulation of anthocyanin-like pigment (purple) around air chambers on the dorsal thallus surface. Scale bars, 1 mm ($n = 8$).

(E) Bright-field and epifluorescence micrographs illustrating the lack of *P. palmivora* ARI-td (red fluorescent) hyphae in pigmented (arrows) areas of TAK1 liverwort thalli at 5 dpi ($n = 8$). Scale bars, 1 mm.

***P. palmivora* Infection Activates *MpMyb14* and a Suite of Flavonoid Biosynthesis Genes**

In angiosperms, the biosynthesis of flavonoids and other polyphenolic compounds derived from phenylalanine and tyrosine (phenylpropanoids) is typically activated by developmental and stress-related programs via MYB transcription factors [33, 34]. Our expression analysis of annotated *M. polymorpha* gene families showing conservation across land plants revealed a strong upregulation of the R2R3-MYB transcription factor *MpMyb14* (Mapoly0073s0038) and several loci associated with flavonoid biosynthesis during infection of *Marchantia* thalli with *P. palmivora*. Previous reports have linked *MpMyb14* expression

with the biosynthesis of polyphenolic or flavonoid-like compounds that include the liverwort-specific anthocyanin Riccionidin A, which appears as a dark red/purple pigment in liverwort thalli during abiotic stress [35–37]. To confirm that *MpMyb14* is induced during oomycete infection, we performed qRT-PCR analysis of mock- and *P. palmivora* ARI-td-treated TAK1 thalli over a 4-day infection time course. A significant induction of *MpMyb14* transcripts was observed from 2 to 4 dpi in *P. palmivora*-infected thalli relative to mock-treated controls (Figure 4A). Next, we compared our infection RNA-seq data (4-dpi time point) with that of *MpMyb14*-overexpressing plants [37] to assess the extent to which *MpMyb14* may influence the

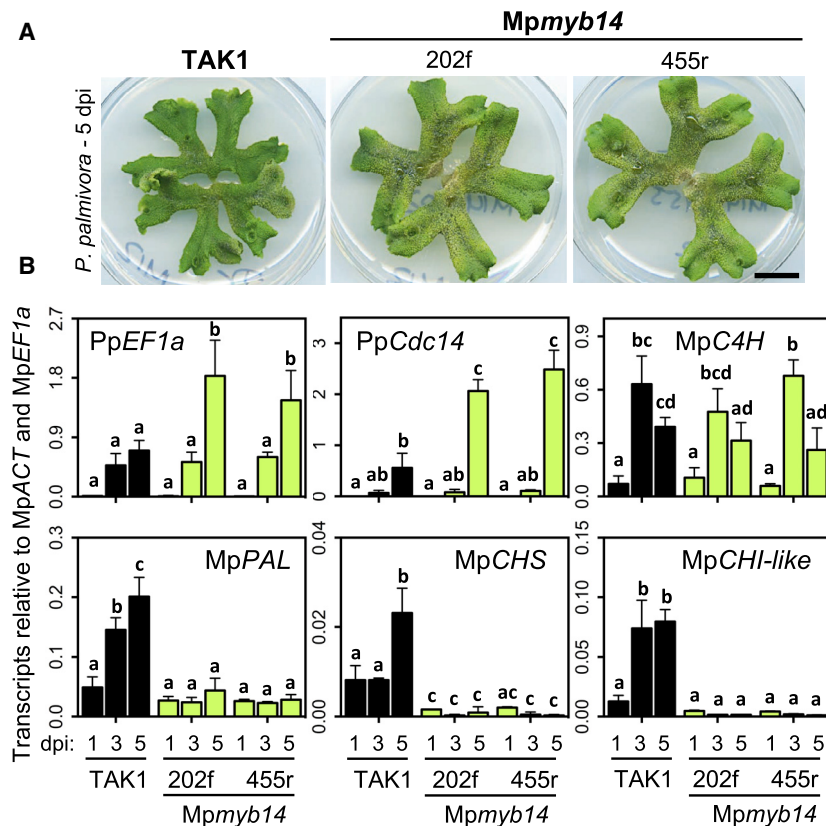


Figure 5. MpmMyb14-Dependent Regulation of Flavonoid Biosynthesis Genes Is Required for Liverwort Resistance to Oomycete Infection

(A) Macroscopic phenotypes of 3-week-old *MpmMyb14* mutant (202f and 455r) and wild-type (TAK1) liverworts 5 dpi with *P. palmivora* ARI-td. Scale bar, 1 cm (n = 5). (B) Quantification of *P. palmivora* biomass (PpEF1a), sporulation (PpCdc14), and phenylpropanoid biosynthesis genes (MpC4H, Mapoly0163s0018; MpPAL, Mapoly0005s0089; MpCHS, Mapoly0021s0159; MpCHI-like, Mapoly0175s0004) during *P. palmivora* ARI-td infection in wild-type (TAK1) and *MpmMyb14* (202f and 455r) mutant liverworts at 1, 3, and 5 dpi (n = 8 per treatment and time point). Gene expression was quantified relative to the *M. polymorpha* biomass markers MpACT and MpEF1a. Different letters signify statistically significant differences in transcript abundance (ANOVA, Tukey's HSD, p < 0.05). Error bars represent SD.

transcriptional response to pathogen infection in *Marchantia*. This comparison revealed 191 genes commonly activated during pathogen infection (19.7% of all pathogen-induced transcripts) and *MpmMyb14* overexpression (Figure 4B), of which 20 were associated with flavonoid biosynthesis (Data S1). Such *MpmMyb14*-regulated and infection-induced genes included *chalcone synthases* (CHSs), *phenylalanine ammonia lyases* (PALs), *chalcone-flavone isomerase-like* (CHI-like), and *cinnamate-4-hydroxylases* (C4Hs), among other enzymes. Using qRT-PCR analysis, we validated the upregulation of representative flavonoid biosynthesis genes (MpPAL, MpCHS, MpCHI-like, MpC4H) in *P. palmivora*-infected TAK1 relative to mock-treated controls (Figure 4C). Together, these data suggest that *P. palmivora* infection activates the biosynthesis of flavonoids in *Marchantia* thalli. In support of this, we observed the accumulation of dark red/purple pigment in TAK1 thalli infected with *P. palmivora* ARI-td beginning from 4 dpi (Figure 4D). Characteristic anthocyanin-like pigment was most prominently observed around the walls of air chambers and epifluorescence microscopy revealed that *P. palmivora* ARI-td hyphae were largely absent in pigmented areas (Figures 4D and 4F), which suggests that flavonoid biosynthesis may promote resistance to oomycete infection in *Marchantia*.

MpmMyb14 Mutants Lack Oomycete-Induced Phenylpropanoid Biosynthesis Gene Induction and Are Highly Susceptible to *P. palmivora*

To better ascertain the role of *MpmMyb14* during oomycete infection in *Marchantia*, we challenged *MpmMyb14* knockout

mutants [37] and a parental wild-type (TAK1) control with *P. palmivora*. Over a 7-day infection time course, severe disease symptoms quickly developed in *MpmMyb14* mutant lines (202f and 455r) compared to TAK1 (Figure 5A). To further support these observations, we performed qRT-PCR analysis of pathogen transcripts indicative of oomycete biomass (PpEF1a) and sporulation (PpCdc14). Compared to the wild-type control, pathogen biomass and sporulation were significantly higher in both *MpmMyb14* mutants (Figure 5B). Further analysis of *MpmMyb14*-regulated phenylpropanoid or flavonoid biosynthesis gene expression [37] revealed significant reductions in pathogen-induced MpPAL, MpCHS, and MpCHI-like, but not MpC4H, in susceptible *MpmMyb14* knockouts relative to the more resistant TAK1 control (Figure 5B). Collectively, these data identify a strong role for *MpmMyb14* in mediating liverwort resistance to oomycete infection.

The Ectopic Accumulation of MpmMyb14-Regulated Pigment Is Associated with Enhanced Resistance to Oomycete Infection

The enhanced disease susceptibility of *MpmMyb14* mutants and the diminished occurrence of *P. palmivora* hyphae in pigmented areas of TAK1 thalli suggested that flavonoid accumulation suppresses pathogen infection *in planta*. To investigate this further, we ectopically overexpressed *MpmMyb14* in TAK1 *M. polymorpha* liverworts and assessed the impact of anthocyanin overproduction on *P. palmivora* pathogenicity. Our initial efforts to establish constitutive *pro35S:mCitrine-MpmMyb14* overexpression lines yielded highly pigmented plants with stunted growth (Figure S3A), which supports the idea that flavonoid overproduction negatively impacts liverwort growth [35]. To circumvent this issue, we generated heat-shock-inducible *MpmMyb14* expression lines using the *HSP17.8A1* promoter [38, 39]. In our conditions, this promoter demonstrated spurious activation in the absence of heat stress that resulted in a mosaic thallus displaying discrete sectors with pigment accumulation (Figure 6A). We took

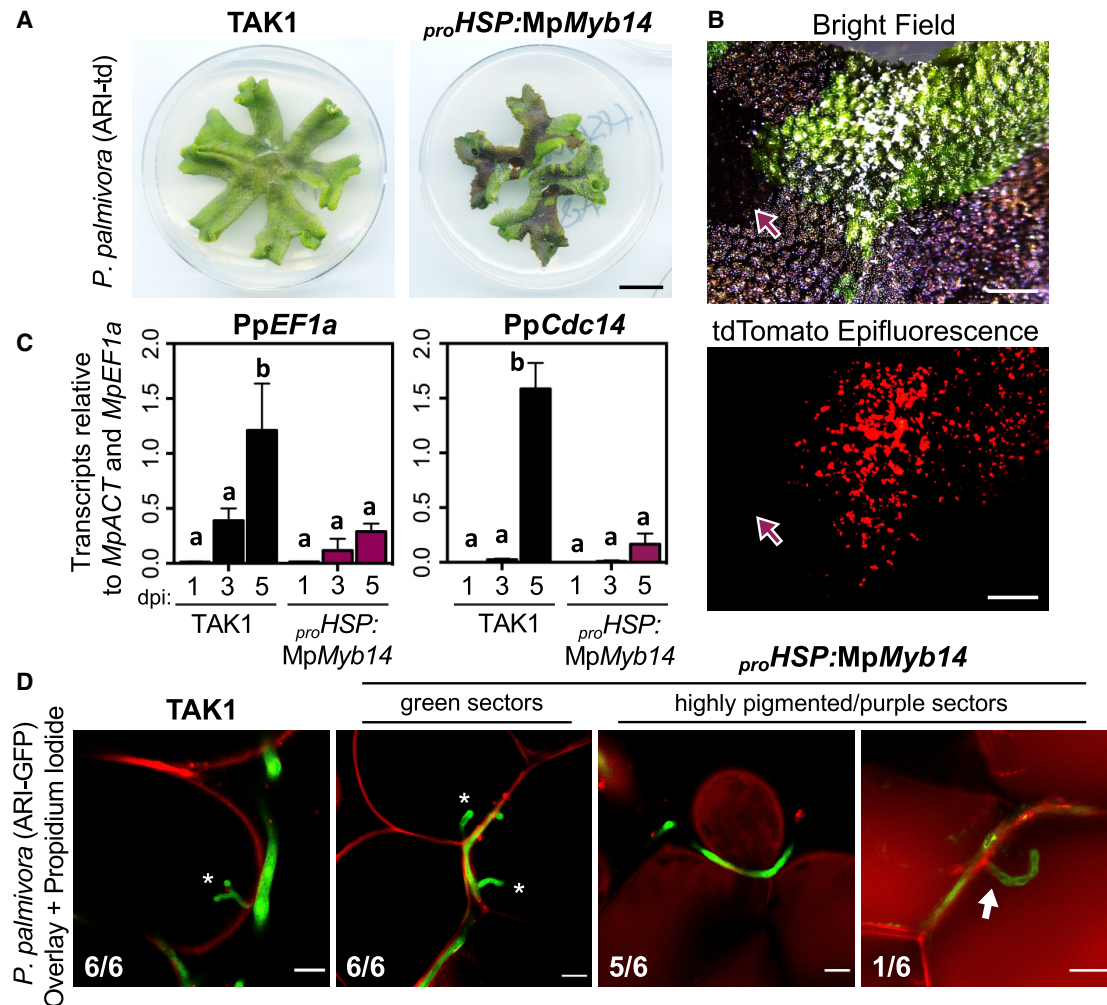


Figure 6. The Ectopic Over-accumulation of MpMyb14-Regulated Phenylpropanoids Enhances Resistance to *P. palmivora*

(A) Macroscopic phenotypes of 3-week-old *proHSP:MpMyb14* and wild-type (TAK1) liverworts 7 dpi with *P. palmivora* ARI-td. Scale bar, 1 cm (n = 8).

(B) Bright-field and epifluorescence micrographs demonstrating the differential colonization of *proHSP:MpMyb14* thalli by *P. palmivora* ARI-td (red fluorescence) at 5 dpi. Pigmented sectors appear dark purple whereas non-pigmented sectors are green. An arrow indicates the site of *P. palmivora* zoospore inoculation in a pigmented sector. Scale bar, 0.1 cm (n = 8).

(C) Quantification of *P. palmivora* biomass (PpEF1a) and sporulation (PpCdc14) marker genes during the colonization of pigmented sectors of *proHSP:MpMyb14* compared to wild-type (TAK1) plants at 1, 3, and 5 dpi (n = 8 plants per time point and treatment). *Phytophthora* marker gene expression was quantified relative to the *M. polymorpha* biomass markers MpACT and MpEF1a. Different letters signify statistically significant differences in transcript abundance (ANOVA, Tukey's HSD, $p < 0.05$). Error bars represent SD.

(D) Confocal fluorescence microscopy demonstrating intracellular colonization phenotypes of TAK1 and green (non-pigmented) versus purple (highly pigmented) sectors of *proHSP:MpMyb14* liverworts infected with *P. palmivora* GFP (3 dpi). Pathogen fluorescence (GFP) is overlaid with propidium iodide staining (red) to discern intra- versus intercellular hyphal growth *in planta*. Branched or digit-type haustoria are denoted with an asterisk whereas invasive hyphae are indicated by an arrow. Occurrence of the observed structures in (n = 6) infected liverworts is denoted per representative image. Scale bars, 10 μ m.

See also Figure S3.

advantage of this phenotype and performed *P. palmivora* infection assays comparing colonization dynamics in pigmented sectors of *proHSP:MpMyb14* plants relative to wild-type TAK1. Pigmented sectors inoculated with *P. palmivora* ARI-td zoospores remained relatively healthy over a 6-day infection time course relative to non-pigmented sectors of the same plants or wild-type TAK1 controls (Figures 6A and 6B). The preferential colonization of non-pigmented sectors of *proHSP:MpMyb14* plants was further supported by epifluorescence microscopy, which revealed extensive hyphal growth and sporulation of red

fluorescent *P. palmivora* in non-pigmented sectors relative to pigmented inoculation sites (Figure 6B). In support of these observations, qRT-PCR analysis revealed a significant reduction in pathogen biomass (PpEF1a) and sporulation-associated (PpCdc14) transcripts in pigmented sectors of *proHSP:MpMyb14* compared to wild-type TAK1 controls by 5 dpi (Figure 6C). To address whether MpMyb14-overexpressing cells establish a hostile environment for invasive hyphae, we assessed whether pigmented sectors of *proHSP:MpMyb14* liverworts display enhanced resistance to intracellular colonization

compared to non-pigmented sectors or wild-type controls. Initial experiments using *P. palmivora* ARI-td suggested that intracellular infection structures were not established in pigmented sectors of *proHSP:MpMyb14* relative to non-pigmented sectors and wild-type controls (Figure S3B). To further support this result, we generated a GFP-expressing *P. palmivora* strain (ARI-GFP) for compatible use with propidium iodide staining to better discriminate between intra- and intercellular hyphal growth. In our experiments, propidium iodide fluorescence overlapped with phenylpropanoid metabolite autofluorescence in pigmented tissues (Figure S3C) but nevertheless discriminated between intra- and intercellular compartments. As expected, *P. palmivora* ARI-GFP was highly infectious and developed intracellular infection structures in TAK1 as well as non-pigmented *proHSP:MpMyb14* sectors (Figure 6D). Similar to previous observations using *P. palmivora* ARI-td, intercellular hyphal growth was predominantly observed in pigmented sectors of *proHSP:MpMyb14* (5/6 infection sites); however, a single intracellular hyphal invasion event was observed in a single infection site (1/6) in only one of three experimental replicates (Figure 6D). Collectively, the data demonstrate that MpMyb14-regulated flavonoid and phenylpropanoid accumulation is associated with enhanced resistance to *P. palmivora* infection in *Marchantia*.

DISCUSSION

In this study, we demonstrate that the early-divergent model liverwort *M. polymorpha* activates features of an evolutionarily conserved plant defense response during colonization by the pathogenic oomycete *P. palmivora*. This response was characterized by the induction of a number of gene families classically associated with defense, such as PR proteins, stress-associated enzymes, transcription factors, and cellular trafficking machinery. Whereas several studies have demonstrated the upregulation of PR genes during angiosperm-pathogen interactions, limited evidence supports their conserved activation in distantly related plant lineages. Transcriptomic and phylogenetic analyses identified conserved PR genes in gymnosperms (*Pinus tecunumanii* and *Pinus patula*) that were transcriptionally induced during interactions with the phytopathogenic fungus *Fusarium circinatum* [30]. Homologs of most PR families were represented in the genomes of selected gymnosperms and early-diverging land plants (lycophytes, bryophytes), with the exception of the PR12 (defensin) and PR13 (thionin) proteins that appear only in angiosperms [30]. Our analysis of *Marchantia* PR genes also failed to identify PR12/PR13 homologs, which is consistent with the idea that these genes evolved later in the evolution of land plants. Additional studies have revealed the pathogen-induced expression of PR1/PR10 homologs in the moss *P. patens* [40, 41] and the differential regulation of *Azolla filiculoides* (water fern) PR5/PR12 homologs in response to the defense hormone methyl-salicylate [42]. Together, these works suggest a conserved role for PR gene families in mediating responses to pathogens throughout the green plant lineage, with MpPR6a (protease inhibitor) and MpPRX/PR9 (peroxidase) representing highly inducible members of the *M. polymorpha* PR complement. How these loci functionally contribute to this interaction is currently unknown; however, expression profiles revealed by promoter-GUS fusions suggest that MpPR6a (this

work) may act in a more localized manner compared to MpPRX/PR9 [26]. It was previously suggested that the moss *Amblystegium serpens* employs a form of systemic acquired resistance (SAR) in response to localized MAMP treatments [43]; however, it remains to be seen whether this response is observed during pathogen infection and whether functionally similar analogs of mobile angiosperm SAR signals are produced in early-diverging lineages.

Adjustments in the *Marchantia* transcriptome caused by oomycete colonization include the differential regulation of transcription factor families conserved across land plants and algal predecessors. The complement of pathogen-responsive transcription factors in *Marchantia* contained several families associated with responses to microbial colonization in angiosperms (WRKY, GRAS, NAC, ERF, bHLH, MYB), which may hint at ancestral roles for these families in biotic and/or cellular stress tolerance. GRAS transcription factors are broadly implicated in the control of developmental programs and symbiotic plant-microbe interactions in angiosperms [44], with recent phylogenetic efforts demonstrating the conservation of key symbiosis-related GRAS clades in bryophytes [19, 45]. Two *Marchantia* GRAS transcription factors were induced during infection with *P. palmivora*, which is consistent with previous work demonstrating the upregulation of the GRAS protein RAD1 during the colonization of *Medicago* roots by *P. palmivora* [46]. *Medicago rad1* mutants support similarly reduced levels of detrimental and beneficial microbes compared to wild-type controls, indicative of a regulatory role for RAD1 in controlling the intracellular colonization of plant tissues by microbes [46]. *M. polymorpha* does not support arbuscular mycorrhizal (AM) symbiosis and lacks a clear RAD1 ortholog, unlike other AM-competent liverworts [19, 45]. Whether RAD1 and/or additional GRAS subfamilies (RAM, DELLA, etc.) influence microbial colonization across land plants remains to be clarified and requires further phylogenetic and functional analyses, especially in AM symbiosis-supporting bryophytes such as *Marchantia paleacea* or the hornwort *Anthoceros agrestis* [45, 47]. WRKY transcription factors also represent a key gene family relevant to plant-pathogen interactions in angiosperms that is likely relevant across land plants [48, 49]. Their importance in controlling plant immunity is further exemplified by the incorporation of WRKY domains as decoys coded within plant resistance proteins that monitor for interference of WRKY-mediated immune signaling caused by microbial effector proteins [50]. Such WRKY-domain-containing R proteins are present in several monocot and dicot lineages [51], which suggests a prolonged and/or widespread evolutionary pressure to protect complex WRKY signaling pathways during the expansion of angiosperm lineages. A number of WRKY transcription factors were differentially expressed during colonization of *Marchantia* thalli by *P. palmivora*, which hints at a WRKY-mediated transcriptional response that fails to suppress oomycete colonization. Whether *P. palmivora* effectors manipulate conserved immune signaling modules (directly or indirectly) to promote microbial colonization in *Marchantia* and other land plants remains to be determined, but would begin to explain the success of this broad host-range pathogen in phylogenetically distant plant species.

To better understand the extent to which distantly related plants respond to microbial colonization, we compared the

transcriptional response of *M. polymorpha* liverworts with that of the model angiosperm *N. benthamiana*. Remarkably, and despite millions of years of divergence time on a macroevolutionary timescale, we observed features of a common defense response activated by *P. palmivora* infection in both systems. This included several annotated categories of conserved plant genes involved in cell trafficking and signaling, and most strikingly included enzymes associated with the biosynthesis of phenylpropanoid and flavonoid-like metabolites. Phenylpropanoid-mediated biochemical defenses are commonly deployed during plant-pathogen interactions in angiosperms [52–54] and previous phylogenomic analyses have identified conserved phenylpropanoid metabolism genes in early-diverging land plants [15, 53]. We demonstrated that oomycete colonization induces phenylpropanoid metabolism in *Marchantia* thalli, which included the upregulation of enzymes associated with flavonoid biosynthesis such as PALs, CHSs, CHI-like, and C4Hs. Importantly, these genes are similarly induced in oomycete-colonized angiosperms such as *N. benthamiana* and in moss treated with microbial elicitors [21, 55] or infected with *Pythium irregulare* [40]. Together, these data suggest that land plants have a shared capacity to launch phenylpropanoid-mediated biochemical defenses during infection.

The full complement of defense-related phenylpropanoid metabolites deployed in early-divergent land plants is currently unknown; however, we observed a clear accumulation of red/purple anthocyanidin pigment in oomycete-colonized thalli. Infection-induced pigment accumulation was concomitant with the upregulation of the MYB transcription factor MpMyb14 and a suite of flavonoid biosynthesis genes that were previously identified as MpMyb14-targeted loci important for flavonoid and anthocyanidin (Riccionidin A) biosynthesis [35, 37]. This suggests that the pathogen-induced upregulation of phenylpropanoid metabolites such as Riccionidin A are routed through MpMyb14 in *Marchantia*, which was supported by the ~20% overlap in the transcriptional profiles of oomycete-infected thalli and MpMyb14-overexpressing plants. Previous studies have demonstrated a role for MpMyb14 in activating anthocyanidin accumulation in response to abiotic stressors such as nutrient deprivation, light stress, high NaCl, and exposure to UV-B [35–37]. These studies further demonstrated a protective function for MpMyb14-regulated flavonoids against oxidative stress [37], which provided flavonoid hyper-accumulating MpMyb14-overexpression lines with enhanced tolerance to UV-B exposure [36]. Here, we show that *Mpmyb14* mutants lack oomycete-induced flavonoid/phenylpropanoid biosynthesis gene induction and are more susceptible to *P. palmivora* infection, which suggests a role for flavonoid biosynthesis in liverwort disease resistance. Consistent with this idea, we observed that MpMyb14-associated pigment accumulation provides *Marchantia* thalli with enhanced resistance to *P. palmivora* infection. Pigmented areas of wild-type plants displayed reduced levels of pathogen hyphae and pigmented sectors of MpMyb14-overexpressing thalli supported reduced levels of pathogen growth relative to non-pigmented sectors and wild-type controls. Given that MpMyb14-associated phenylpropanoid metabolites afford thalli with enhanced tolerance to oxidative stress, it is likely that this function is at least partly responsible for the bolstered resistance to *P. palmivora* infection. However, we cannot rule out the possibility that the

complement of MpMyb14-regulated metabolites includes an antimicrobial or cell-wall-strengthening compound that is highly effective against *P. palmivora*. Indeed, pigmented sectors of *proHSP:MpMyb14* liverworts exhibited fewer events of intracellular colonization, which may suggest a role for Riccionidin A in cell-wall-associated defenses. Because MpMyb14 regulates both early and late steps of the phenylpropanoid pathway, specific Riccionidin A biosynthesis mutants are required to understand its role in defense. In angiosperms, a diverse set of phenylpropanoid metabolites (colorless flavonoids, anthocyanin pigments, cinnamic acids, lignins, or lignans, etc.) have demonstrated antimicrobial, antioxidative, and cell-wall-reinforcement activities that contribute to plant resistance against microbial infection [53, 54, 56–58]. Whereas early-divergent land plants belonging to the bryophytes lack lignin, it was recently suggested that the phenol-enriched cuticle and cell wall of the moss *P. patens* may represent an ancestral feature critical to the expansion of plants onto land [59]. Whether pathogen-induced phenylpropanoids contribute to modifications of phenolic *Marchantia* cell walls during infection remains a possibility, as Riccionidin A pigment is predominantly integrated into liverwort cell walls [35, 37] whereas colorless flavonoids similarly regulated by MpMyb14 remain in the cytosol [37]. A suite of dirigent (*DIR*) genes, which have been associated with lignin or lignan biochemistry in angiosperms [60], are upregulated alongside phenylpropanoid biosynthesis genes during oomycete infection and may contribute to chemical complexity in phenolic cell walls of bryophytes. Collectively, these observations suggest that MpMyb14 regulates a suite of phenylpropanoid metabolites that fulfil multiple roles in protecting liverwort thalli from biotic and abiotic stress.

Flavonoid biosynthesis is generally controlled by the MBW (R2R3-MYB, bHLH, WD40) protein complex in angiosperms [33, 34]. In early-diverging plant lineages such as liverworts it is not yet clear whether such a complex exists, but evidence supports the role of certain R2R3-MYB and bHLH transcription factors in regulating flavonoid biosynthesis [35, 37, 61]. Phylogenetic analysis places the *Marchantia* MpMyb14 protein basal to the MYB subgroups SG4–SG7, which generally represent key activators and repressors (SG4) of flavonoid biosynthesis in angiosperms [35]. Because MpMyb14 is a transcriptional activator, it is possible that the ancestral role of this R2R3-MYB lineage was to activate flavonoid biosynthesis, perhaps independent of a conserved MBW complex because MpMyb14 lacks bHLH-interacting domains [35]. Whereas the majority of angiosperms lack the capacity to synthesize Riccionidin A specifically, several R2R3-MYBs have been shown to control a diverse array of flavonoids and/or anthocyanins during development and stress [33, 34, 54]. In *Arabidopsis*, the SG6 MYB PAP1/MYB75 positively regulates anthocyanin accumulation in response to several environmental stimuli [62–65]. PAP1-mediated anthocyanin accumulation has also been linked to the JA signaling pathway, wherein JAZ-mediated repression of PAP1 is lifted upon JA accumulation, leading to pigment accumulation during stress [66]. Because *Marchantia* encodes a conserved COI1-JAZ module responsive to the JA precursor dn-OPDA [24], it is possible that this pathway similarly regulates flavonoid biosynthesis during biotic stress in liverworts. In any case, our study and others demonstrate that the complex regulation of flavonoid biosynthesis by MYB and bHLH transcription factors has deep

evolutionary roots, with functions in stress tolerance that are present even in early-divergent land plants [35–37, 61]. The charophytic algal predecessors of land plants encode phenylpropanoid biosynthesis genes and have a capacity for embryophyte-like stress signaling [67, 68] yet lack orthologs of MpMyb14 and other flavonoid-regulating R2R3-MYB transcription factors [15, 37]. It therefore appears that the evolution of R2R3-MYB-mediated control of an expanding flavonoid/phenylpropanoid metabolite repertoire likely facilitated key advances in plant development (vertical growth) and stress physiology (antimicrobials, sunscreens, antioxidants, etc.) that were essential for the expansion of plant life on land [15, 35, 37, 69].

Evolutionary plant-pathogen interaction studies have typically focused on tightly co-evolving relationships within plant and microbial populations [70]. Here, we took a comparative macroevolutionary approach that identified conserved orthologous plant genes responsive to oomycete infection in early- and late-diverging land plant lineages. This analysis uncovered a set of pathogen-responsive orthologous genes with roles in vesicular trafficking, antimicrobial defenses, transcriptional control, cell signaling, and stress-associated metabolism. Using this knowledge, we identified a conserved role for phenylpropanoid-associated biochemical defenses in mitigating pathogen infection in liverworts, which presents as an ancestral layer of the plant basal defense response that was likely critical for the expansion of plants on land. Collectively, this work provides key evolutionary insight into the nature of early land plant defense strategies that are shared with distantly related lineages. Future studies on host responses to oomycete infection across diverse land plant lineages (lycophods, ferns, gymnosperms) are likely to reveal additional layers of plant immunity that evolved to protect derived land plant features.

STAR★METHODS

Detailed methods are provided in the online version of this paper and include the following:

- [KEY RESOURCES TABLE](#)
- [LEAD CONTACT AND MATERIALS AVAILABILITY](#)
- [EXPERIMENTAL MODEL AND SUBJECT DETAILS](#)
 - Plant Growth Details
 - Pathogen Growth Details
- [METHOD DETAILS](#)
 - Pathogen Infection Assays
 - *Phytophthora palmivora* Transformation
 - Microscopy & Histochemical Staining
 - RNA Isolation, cDNA Synthesis, and qRT-PCR Analysis
 - Proteomics
 - Cloning and *Marchantia* Transformation
 - Library preparation and sequencing
 - Expression analysis
 - Orthology analysis
- [QUANTIFICATION AND STATISTICAL ANALYSIS](#)

SUPPLEMENTAL INFORMATION

Supplemental Information can be found online at <https://doi.org/10.1016/j.cub.2019.05.078>.

ACKNOWLEDGMENTS

We thank Anne Harzen for support with proteomics efforts, Edwige Moyroud (Sainsbury Laboratory, Cambridge) for commenting on an earlier draft of the manuscript, and Edouard Evangelisti for advice on *Phytophthora* transformation. For additional critical and technical support, we thank Natalia Guayazan Palacios and all members of the Schornack group. This work was funded by the Gatsby Charitable Foundation (GAT3395/GLD), Royal Society (UF160413, RGF\EA\180002), BBSRC OpenPlant initiative (BB/L014130/1), Natural Environment Research Council (NERC; NE/N00941X/1), and a Natural Sciences and Engineering Research Council of Canada (NSERC) postdoctoral fellowship (to P.C.). Proteomics work performed in the Nakagami lab was supported by the Max-Planck-Gesellschaft.

AUTHOR CONTRIBUTIONS

P.C., A.G., and S.S. designed research; P.C., A.G., D.J.H., A.J.B., and S.C.S. performed research; P.C., A.G., S.C.S., H.N., and S.S. analyzed data; S.C.S. and H.N. performed proteomic analysis; and P.C. and S.S. wrote the paper with technical contributions from A.G. and S.C.S.

DECLARATION OF INTERESTS

The authors declare no competing interests.

Received: February 5, 2019

Revised: April 28, 2019

Accepted: May 31, 2019

Published: July 11, 2019

REFERENCES

1. Remy, W., Taylor, T.N., Hass, H., and Kerp, H. (1994). Four hundred-million-year-old vesicular arbuscular mycorrhizae. *Proc. Natl. Acad. Sci. USA* *91*, 11841–11843.
2. Taylor, T.N., Remy, W., Hass, H., and Kerp, H. (1995). Fossil arbuscular mycorrhizae from the Early Devonian. *Mycologia* *87*, 560–573.
3. Taylor, T.N., Krings, M., and Kerp, H. (2006). *Hassiaella monospora* gen. et sp. nov., a microfungus from the 400 million year old Rhynie chert. *Mycol. Res.* *110*, 628–632.
4. Strullu-Derrien, C. (2018). Fossil filamentous microorganisms associated with plants in early terrestrial environments. *Curr. Opin. Plant Biol.* *44*, 122–128.
5. Krings, M., Taylor, T.N., Hass, H., Kerp, H., Dotzler, N., and Hermsen, E.J. (2007). Fungal endophytes in a 400-million-yr-old land plant: infection pathways, spatial distribution, and host responses. *New Phytol.* *174*, 648–657.
6. Boller, T., and Felix, G. (2009). A renaissance of elicitors: perception of microbe-associated molecular patterns and danger signals by pattern-recognition receptors. *Annu. Rev. Plant Biol.* *60*, 379–406.
7. Macho, A.P., and Zipfel, C. (2014). Plant PRRs and the activation of innate immune signaling. *Mol. Cell* *54*, 263–272.
8. Cui, H., Tsuda, K., and Parker, J.E. (2015). Effector-triggered immunity: from pathogen perception to robust defense. *Annu. Rev. Plant Biol.* *66*, 487–511.
9. Bednarek, P. (2012). Chemical warfare or modulators of defence responses—the function of secondary metabolites in plant immunity. *Curr. Opin. Plant Biol.* *15*, 407–414.
10. Meng, X., and Zhang, S. (2013). MAPK cascades in plant disease resistance signaling. *Annu. Rev. Phytopathol.* *51*, 245–266.
11. Morris, J.L., Puttick, M.N., Clark, J.W., Edwards, D., Kenrick, P., Pressel, S., Wellman, C.H., Yang, Z., Schneider, H., and Donoghue, P.C.J. (2018). The timescale of early land plant evolution. *Proc. Natl. Acad. Sci. USA* *115*, E2274–E2283.
12. Puttick, M.N., Morris, J.L., Williams, T.A., Cox, C.J., Edwards, D., Kenrick, P., Pressel, S., Wellman, C.H., Schneider, H., Pisani, D., and Donoghue,

- P.C.J. (2018). The interrelationships of land plants and the nature of the ancestral embryophyte. *Curr. Biol.* **28**, 733–745.e2.
13. de Sousa, F., Foster, P.G., Donoghue, P.C.J., Schneider, H., and Cox, C.J. (2019). Nuclear protein phylogenies support the monophyly of the three bryophyte groups (Bryophyta Schimp.). *New Phytol.* **222**, 565–575.
 14. Rensing, S.A., Lang, D., Zimmer, A.D., Terry, A., Salamov, A., Shapiro, H., Nishiyama, T., Perroud, P.-F., Lindquist, E.A., Kamisugi, Y., et al. (2008). The *Physcomitrella* genome reveals evolutionary insights into the conquest of land by plants. *Science* **319**, 64–69.
 15. Bowman, J.L., Kohchi, T., Yamato, K.T., Jenkins, J., Shu, S., Ishizaki, K., Yamaoka, S., Nishihama, R., Nakamura, Y., Berger, F., et al. (2017). Insights into land plant evolution garnered from the *Marchantia polymorpha* genome. *Cell* **171**, 287–304.e15.
 16. Ponce de León, I., and Montesano, M. (2017). Adaptation mechanisms in the evolution of moss defenses to microbes. *Front. Plant Sci.* **8**, 366.
 17. Carella, P., and Schornack, S. (2018). Manipulation of bryophyte hosts by pathogenic and symbiotic microbes. *Plant Cell Physiol.* **59**, 651–660.
 18. de Vries, S., de Vries, J., von Dahlen, J.K., Gould, S.B., Archibald, J.M., Rose, L.E., and Slamovits, C.H. (2018). On plant defense signaling networks and early land plant evolution. *Commun. Integr. Biol.* **11**, 1–14.
 19. Delaux, P.-M., Radhakrishnan, G.V., Jayaraman, D., Cheema, J., Malbreil, M., Volkening, J.D., Sekimoto, H., Nishiyama, T., Melkonian, M., Pokorny, L., et al. (2015). Algal ancestor of land plants was preadapted for symbiosis. *Proc. Natl. Acad. Sci. USA* **112**, 13390–13395.
 20. Field, K.J., and Pressel, S. (2018). Unity in diversity: structural and functional insights into the ancient partnerships between plants and fungi. *New Phytol.* **220**, 996–1011.
 21. Bressendorff, S., Azevedo, R., Kenchappa, C.S., Ponce de León, I., Olsen, J.V., Rasmussen, M.W., Erbs, G., Newman, M.-A., Petersen, M., and Mundy, J. (2016). An innate immunity pathway in the moss *Physcomitrella patens*. *Plant Cell* **28**, 1328–1342.
 22. Reboledo, G., Del Campo, R., Alvarez, A., Montesano, M., Mara, H., and Ponce de León, I. (2015). *Physcomitrella patens* activates defense responses against the pathogen *Colletotrichum gloeosporioides*. *Int. J. Mol. Sci.* **16**, 22280–22298.
 23. Overdijk, E.J.R., De Keijzer, J., De Groot, D., Schoina, C., Bouwmeester, K., Ketelaar, T., and Govers, F. (2016). Interaction between the moss *Physcomitrella patens* and *Phytophthora*: a novel pathosystem for live-cell imaging of subcellular defence. *J. Microsc.* **263**, 171–180.
 24. Monte, I., Ishida, S., Zamarreño, A.M., Hamberg, M., Franco-Zorrilla, J.M., García-Casado, G., Gouhier-Darimont, C., Reymond, P., Takahashi, K., García-Mina, J.M., et al. (2018). Ligand-receptor co-evolution shaped the jasmonate pathway in land plants. *Nat. Chem. Biol.* **14**, 480–488.
 25. Nelson, J.M., Hauser, D.A., Hinson, R., and Shaw, A.J. (2018). A novel experimental system using the liverwort *Marchantia polymorpha* and its fungal endophytes reveals diverse and context-dependent effects. *New Phytol.* **218**, 1217–1232.
 26. Carella, P., Gogleva, A., Tomaselli, M., Alfs, C., and Schornack, S. (2018). *Phytophthora palmivora* establishes tissue-specific intracellular infection structures in the earliest divergent land plant lineage. *Proc. Natl. Acad. Sci. USA* **115**, E3846–E3855.
 27. van Loon, L.C., Pierpoint, W.S., Boller, Th., and Conejero, V. (1994). Recommendations for naming plant pathogenesis-related proteins. *Plant Mol. Biol. Report.* **12**, 245–264.
 28. Sels, J., Mathys, J., De Coninck, B.M.A., Cammue, B.P.A., and De Bolle, M.F.C. (2008). Plant pathogenesis-related (PR) proteins: a focus on PR peptides. *Plant Physiol. Biochem.* **46**, 941–950.
 29. Ali, S., Ganai, B.A., Kamili, A.N., Bhat, A.A., Mir, Z.A., Bhat, J.A., Tyagi, A., Islam, S.T., Mushtaq, M., Yadav, P., et al. (2018). Pathogenesis-related proteins and peptides as promising tools for engineering plants with multiple stress tolerance. *Microbiol. Res.* **212–213**, 29–37.
 30. Visser, E.A., Wegrzyn, J.L., Myburg, A.A., and Naidoo, S. (2018). Defence transcriptome assembly and pathogenesis related gene family analysis in *Pinus tecunumanii* (low elevation). *BMC Genomics* **19**, 632.
 31. Evangelisti, E., Gogleva, A., Hainaux, T., Doumane, M., Tulin, F., Quan, C., Yunusov, T., Floch, K., and Schornack, S. (2017). Time-resolved dual transcriptomics reveal early induced *Nicotiana benthamiana* root genes and conserved infection-promoting *Phytophthora palmivora* effectors. *BMC Biol.* **15**, 39.
 32. Emms, D.M., and Kelly, S. (2015). OrthoFinder: solving fundamental biases in whole genome comparisons dramatically improves orthogroup inference accuracy. *Genome Biol.* **16**, 157.
 33. Liu, J., Osbourn, A., and Ma, P. (2015). MYB transcription factors as regulators of phenylpropanoid metabolism in plants. *Mol. Plant* **8**, 689–708.
 34. Xu, W., Dubos, C., and Lepiniec, L. (2015). Transcriptional control of flavonoid biosynthesis by MYB-bHLH-WDR complexes. *Trends Plant Sci.* **20**, 176–185.
 35. Albert, N.W., Thrimawithana, A.H., McGhie, T.K., Clayton, W.A., Deroles, S.C., Schwinn, K.E., Bowman, J.L., Jordan, B.R., and Davies, K.M. (2018). Genetic analysis of the liverwort *Marchantia polymorpha* reveals that R2R3MYB activation of flavonoid production in response to abiotic stress is an ancient character in land plants. *New Phytol.* **218**, 554–566.
 36. Clayton, W.A., Albert, N.W., Thrimawithana, A.H., McGhie, T.K., Deroles, S.C., Schwinn, K.E., Warren, B.A., McLachlan, A.R.G., Bowman, J.L., Jordan, B.R., and Davies, K.M. (2018). UVR8-mediated induction of flavonoid biosynthesis for UVB tolerance is conserved between the liverwort *Marchantia polymorpha* and flowering plants. *Plant J.* **96**, 503–517.
 37. Kubo, H., Nozawa, S., Hiwatashi, T., Kondou, Y., Nakabayashi, R., Mori, T., Saito, K., Takanashi, K., Kohchi, T., and Ishizaki, K. (2018). Biosynthesis of riccionidins and marchantins is regulated by R2R3-MYB transcription factors in *Marchantia polymorpha*. *J. Plant Res.* **131**, 849–864.
 38. Nishihama, R., Ishida, S., Urawa, H., Kamei, Y., and Kohchi, T. (2016). Conditional gene expression/deletion systems for *Marchantia polymorpha* using its own heat-shock promoter and Cre/loxP-mediated site-specific recombination. *Plant Cell Physiol.* **57**, 271–280.
 39. Ishizaki, K., Nishihama, R., Ueda, M., Inoue, K., Ishida, S., Nishimura, Y., Shikanai, T., and Kohchi, T. (2015). Development of Gateway binary vector series with four different selection markers for the liverwort *Marchantia polymorpha*. *PLoS ONE* **10**, e0138876.
 40. Oliver, J.P., Castro, A., Gaggero, C., Cascón, T., Schmelz, E.A., Castresana, C., and Ponce de León, I. (2009). Pythium infection activates conserved plant defense responses in mosses. *Planta* **230**, 569–579.
 41. Castro, A., Vidal, S., and Ponce de León, I. (2016). Moss pathogenesis-related-10 protein enhances resistance to *Pythium irregulare* in *Physcomitrella patens* and *Arabidopsis thaliana*. *Front. Plant Sci.* **7**, 580.
 42. de Vries, S., de Vries, J., Teschke, H., von Dahlen, J.K., Rose, L.E., and Gould, S.B. (2018). Jasmonic and salicylic acid response in the fern *Azolla filiculoides* and its cyanobiont. *Plant Cell Environ.* **41**, 2530–2548.
 43. Winter, P.S., Bowman, C.E., Villani, P.J., Dolan, T.E., and Hauck, N.R. (2014). Systemic acquired resistance in moss: further evidence for conserved defense mechanisms in plants. *PLoS ONE* **9**, e0101880.
 44. Hirsch, S., and Oldroyd, G.E.D. (2009). GRAS-domain transcription factors that regulate plant development. *Plant Signal. Behav.* **4**, 698–700.
 45. Grosche, C., Genau, A.C., and Rensing, S.A. (2018). Evolution of the symbiosis-specific GRAS regulatory network in bryophytes. *Front. Plant Sci.* **9**, 1621.
 46. Rey, T., Bonhomme, M., Chatterjee, A., Gavrin, A., Toulotte, J., Yang, W., André, O., Jacquet, C., and Schornack, S. (2017). The *Medicago truncatula* GRAS protein RAD1 supports arbuscular mycorrhiza symbiosis and *Phytophthora palmivora* susceptibility. *J. Exp. Bot.* **68**, 5871–5881.
 47. Vigneron, N., Radhakrishnan, G.V., and Delaux, P.-M. (2018). What have we learnt from studying the evolution of the arbuscular mycorrhizal symbiosis? *Curr. Opin. Plant Biol.* **44**, 49–56.
 48. Pandey, S.P., and Somssich, I.E. (2009). The role of WRKY transcription factors in plant immunity. *Plant Physiol.* **150**, 1648–1655.
 49. Rushton, P.J., Somssich, I.E., Ringler, P., and Shen, Q.J. (2010). WRKY transcription factors. *Trends Plant Sci.* **15**, 247–258.

50. Sarris, P.F., Duxbury, Z., Huh, S.U., Ma, Y., Segonzac, C., Sklenar, J., Derbyshire, P., Cevik, V., Rallapalli, G., Saucet, S.B., et al. (2015). A plant immune receptor detects pathogen effectors that target WRKY transcription factors. *Cell* **167**, 1089–1100.
51. Sarris, P.F., Cevik, V., Dagdas, G., Jones, J.D.G., and Krasileva, K.V. (2016). Comparative analysis of plant immune receptor architectures uncovers host proteins likely targeted by pathogens. *BMC Biol.* **14**, 8.
52. Dixon, R.A., Achnine, L., Kota, P., Liu, C.-J., Reddy, M.S.S., and Wang, L. (2002). The phenylpropanoid pathway and plant defence—a genomics perspective. *Mol. Plant Pathol.* **3**, 371–390.
53. Naoumkina, M.A., Zhao, Q., Gallego-Giraldo, L., Dai, X., Zhao, P.X., and Dixon, R.A. (2010). Genome-wide analysis of phenylpropanoid defence pathways. *Mol. Plant Pathol.* **11**, 829–846.
54. Falcone Ferreyra, M.L., Rius, S.P., and Casati, P. (2012). Flavonoids: biosynthesis, biological functions, and biotechnological applications. *Front. Plant Sci.* **3**, 222.
55. Alvarez, A., Montesano, M., Schmelz, E., and Ponce de León, I. (2016). Activation of shikimate, phenylpropanoid, oxylipins, and auxin pathways in *Pectobacterium carotovorum* elicitors-treated moss. *Front. Plant Sci.* **7**, 328.
56. Cushnie, T.P.T., and Lamb, A.J. (2005). Antimicrobial activity of flavonoids. *Int. J. Antimicrob. Agents* **26**, 343–356.
57. Cisowska, A., Wojnicz, D., and Hendrich, A.B. (2011). Anthocyanins as antimicrobial agents of natural plant origin. *Nat. Prod. Commun.* **6**, 149–156.
58. Piasecka, A., Jedrzejczak-Rey, N., and Bednarek, P. (2015). Secondary metabolites in plant innate immunity: conserved function of divergent chemicals. *New Phytol.* **206**, 948–964.
59. Renault, H., Alber, A., Horst, N.A., Basilio Lopes, A., Fich, E.A., Kriegshauser, L., Wiedemann, G., Ullmann, P., Herrgott, L., Erhardt, M., et al. (2017). A phenol-enriched cuticle is ancestral to lignin evolution in land plants. *Nat. Commun.* **8**, 14713.
60. Paniagua, C., Bilkova, A., Jackson, P., Dabravolski, S., Riber, W., Didi, V., Houser, J., Gigli-Bisceglia, N., Wimmerova, M., Budínská, E., et al. (2017). Dirigent proteins in plants: modulating cell wall metabolism during abiotic and biotic stress exposure. *J. Exp. Bot.* **68**, 3287–3301.
61. Wu, Y.F., Zhao, Y., Liu, X.Y., Gao, S., Cheng, A.X., and Lou, H.X. (2018). A bHLH transcription factor regulates bisbibenzyl biosynthesis in the liverwort *Plagiochasma appendiculatum*. *Plant Cell Physiol.* **59**, 1187–1199.
62. Lillo, C., Lea, U.S., and Ruoff, P. (2008). Nutrient depletion as a key factor for manipulating gene expression and product formation in different branches of the flavonoid pathway. *Plant Cell Environ.* **31**, 587–601.
63. Shan, X., Zhang, Y., Peng, W., Wang, Z., and Xie, D. (2009). Molecular mechanism for jasmonate-induction of anthocyanin accumulation in *Arabidopsis*. *J. Exp. Bot.* **60**, 3849–3860.
64. Li, S., Wang, W., Gao, J., Yin, K., Wang, R., Wang, C., Petersen, M., Mundy, J., and Qiu, J.-L. (2016). MYB75 phosphorylation by MPK4 is required for light-induced anthocyanin accumulation in *Arabidopsis*. *Plant Cell* **28**, 2866–2883.
65. Wersch, R.V., Gao, F., and Zhang, Y. (2018). Mitogen-activated protein kinase kinase 6 negatively regulates anthocyanin induction in *Arabidopsis*. *Plant Signal. Behav.* **13**, e1526000.
66. Boter, M., Golz, J.F., Giménez-Ibañez, S., Fernández-Barbero, G., Franco-Zorrilla, J.M., and Solano, R. (2015). FILAMENTOUS FLOWER is a direct target of JAZ3 and modulates responses to jasmonate. *Plant Cell* **27**, 3160–3174.
67. de Vries, J., de Vries, S., Slamovits, C.H., Rose, L.E., and Archibald, J.M. (2017). How embryophytic is the biosynthesis of phenylpropanoids and their derivatives in streptophyte algae? *Plant Cell Physiol.* **58**, 934–945.
68. de Vries, J., Curtis, B.A., Gould, S.B., and Archibald, J.M. (2018). Embryophyte stress signaling evolved in the algal progenitors of land plants. *Proc. Natl. Acad. Sci. USA* **115**, E3471–E3480.
69. Tohge, T., Watanabe, M., Hoefgen, R., and Fernie, A.R. (2013). The evolution of phenylpropanoid metabolism in the green lineage. *Crit. Rev. Biochem. Mol. Biol.* **48**, 123–152.
70. Upson, J.L., Zess, E.K., Bialas, A., Wu, C.H., and Kamoun, S. (2018). The coming of age of EvoMPMI: evolutionary molecular plant-microbe interactions across multiple timescales. *Curr. Opin. Plant Biol.* **44**, 108–116.
71. Ali, S.S., Shao, J., Lary, D.J., Kronmiller, B., Shen, D., Strem, M.D., Amoako-Attah, I., Akrofi, A.Y., Begoude, B.A.D., Ten Hoopen, G.M., et al. (2017). *Phytophthora megakarya* and *Phytophthora palmivora*, closely related causal agents of cacao black pod rot, underwent increases in genome sizes and gene numbers by different mechanisms. *Genome Biol. Evol.* **9**, 536–557.
72. Le Febvre, R., O'Boyle, B., Moscou, M.J., and Schornack, S. (2016). Colonization of barley by the broad-host hemibiotrophic pathogen *Phytophthora palmivora* uncovers a leaf development-dependent involvement of *Mlo*. *Mol. Plant Microbe Interact.* **29**, 385–395.
73. Koressaar, T., and Remm, M. (2007). Enhancements and modifications of primer design program Primer3. *Bioinformatics* **23**, 1289–1291.
74. Untergasser, A., Cutcutache, I., Koressaar, T., Ye, J., Faircloth, B.C., Remm, M., and Rozen, S.G. (2012). Primer3—new capabilities and interfaces. *Nucleic Acids Res.* **40**, e115.
75. Cox, J., and Mann, M. (2008). MaxQuant enables high peptide identification rates, individualized p.p.b.-range mass accuracies and proteome-wide protein quantification. *Nat. Biotechnol.* **26**, 1367–1372.
76. Tyanova, S., Temu, T., and Cox, J. (2016). The MaxQuant computational platform for mass spectrometry-based shotgun proteomics. *Nat. Protoc.* **11**, 2301–2319.
77. Love, M.I., Huber, W., and Anders, S. (2014). Moderated estimation of fold change and dispersion for RNA-seq data with DESeq2. *Genome Biol.* **15**, 550.
78. Dobin, A., Davis, C.A., Schlesinger, F., Drenkow, J., Zaleski, C., Jha, S., Batut, P., Chaisson, M., and Gingeras, T.R. (2013). STAR: ultrafast universal RNA-seq aligner. *Bioinformatics* **29**, 15–21.
79. Liao, Y., Smyth, G.K., and Shi, W. (2014). featureCounts: an efficient general purpose program for assigning sequence reads to genomic features. *Bioinformatics* **30**, 923–930.
80. Ah-Fong, A.M.V., and Judelson, H.S. (2011). Vectors for fluorescent protein tagging in *Phytophthora*: tools for functional genomics and cell biology. *Fungal Biol.* **115**, 882–890.
81. Rey, T., Chatterjee, A., Buttay, M., Toulotte, J., and Schornack, S. (2015). *Medicago truncatula* symbiosis mutants affected in the interaction with a biotrophic root pathogen. *New Phytol.* **206**, 497–500.
82. Saint-Marcoux, D., Proust, H., Dolan, L., and Langdale, J.A. (2015). Identification of reference genes for real-time quantitative PCR experiments in the liverwort *Marchantia polymorpha*. *PLoS ONE* **10**, e0118678.
83. Borner, G.H.H., and Fielding, A.B. (2014). Using in-solution digestion, peptide fractionation, and a Q Exactive mass spectrometer to analyze the proteome of clathrin-coated vesicles. *Cold Spring Harb. Protoc.* **2014**, 1192–1195.
84. Kubota, A., Ishizaki, K., Hosaka, M., and Kohchi, T. (2013). Efficient *Agrobacterium*-mediated transformation of the liverwort *Marchantia polymorpha* using regenerating thalli. *Biosci. Biotechnol. Biochem.* **77**, 167–172.

STAR★METHODS

KEY RESOURCES TABLE

REAGENT or RESOURCE	SOURCE	IDENTIFIER
Bacterial and Virus Strains		
<i>E. coli</i> TOP10 chemically competent cells	Invitrogen	Cat#C404006
<i>Agrobacterium tumefaciens</i> GV3101 (pMP90)	Our laboratory collection	N/A
Chemicals, Peptides, and Recombinant Proteins		
PureLink Plant RNA Reagent	ThermoFisher	Cat#12322012
SuperScript II reverse transcriptase	ThermoFisher	Cat#18064014
RNase OUT ribonuclease inhibitor	ThermoFisher	Cat#10777019
Roche SYBR mix	Roche Life Science	Cat#4887352001
Gateway LR clonase II enzyme mix	ThermoFisher	Cat#11791020
MS-media + B5	Duchefa Biochemie	Cat#M0231
Plant agar	Duchefa Biochemie	Cat#P1001
Cefotaxime sodium salt	Sigma-Aldrich	Cat#C7039
Hygromycin B	Melford	Cat#H7502
Chlorsulfuron	Sigma-Aldrich	Cat#34322
G418	Melford	Cat#G0175
carbenicillin	Sigma-Aldrich	Cat#C3416
X-GlcA	Melford	Cat#MB1021
Propidium iodide	Sigma-Aldrich	Cat#P4170
Phosphatase Inhibitor Cocktail 3	Sigma-Aldrich	Cat#P0044-5ML
Phosphatase Inhibitor Cocktail 2	Sigma-Aldrich	Cat#P5726-5ML
Critical Commercial Assays		
QIAprep spin miniprep kit	QIAGEN	Cat#27106
Turbo DNA-free kit	Invitrogen	Cat#AM1907
TruSeq RNA Library Prep Kit v2	Illumina	Cat#RS-122-2001
Deposited Data		
Raw sequencing data: <i>Marchantia polymorpha</i>	This study	NCBI SRA: PRJNA397637
Raw sequencing data: <i>Nicotiana benthamiana</i>	This study	NCBI SRA: PRJNA503573
<i>Marchantia polymorpha</i> reference genome v3.1	[15]	http://marchantia.info/
<i>Nicotiana benthamiana</i> reference genome v1.0.1	SolGenomics Network	https://solgenomics.net/organism/Nicotiana_benthamiana/genome
<i>Phytophthora palmivora</i> reference proteome	[71]	BioProject: PRJNA318026
Raw proteomics data	This study	PRIDE: PXD012076
Experimental Models: Organisms/Strains		
<i>Marchantia polymorpha</i> TAK1	Prof. Jim Haseloff, University of Cambridge	N/A
<i>pro</i> MpPR6a:GUS	This study	N/A
<i>pro</i> MpPR6a:tdTomato-NLS	This study	N/A
<i>pro</i> MpPRX:tdTomato-NLS	This study	N/A
<i>pro</i> 35S:mCitrine-FLAG-MpMyb14	This study	N/A
<i>pro</i> HSP:FLAG-MpMyb14	This study	N/A
Mpmyb14-202f	[37]	N/A
Mpmyb14-455r	[37]	N/A
<i>Nicotiana benthamiana</i>	Our laboratory collection	N/A
<i>Phytophthora palmivora</i> ARI-tdTomato	[72]	N/A
<i>Phytophthora palmivora</i> ARI-GFP	This study	N/A
<i>Phytophthora palmivora</i> LILI-YFP-KDEL	[31]	N/A

(Continued on next page)

Continued

REAGENT or RESOURCE	SOURCE	IDENTIFIER
Oligonucleotides		
A list of all oligonucleotides used in this study can be found in Table S1	This study	N/A
Recombinant DNA		
pMpGWB104	[39]	Addgene Cat#68558
pMpGWB105	[39]	Addgene Cat#68559
pMpGW132	[39]	Addgene Cat#68586
pMpGWB316	[39]	Addgene Cat#68644
<i>pro</i> MpPR6a:tdTomato-NLS	This study	N/A
<i>pro</i> MpPR6a:GUS	This study	N/A
<i>pro</i> MpPRX:tdTomato-NLS	This study	N/A
<i>pro</i> 35S:FLAG-MpMyb14	This study	N/A
<i>pro</i> HSP:FLAG-MpMyb14	This study	N/A
pENTR-proMpPRX	[26]	N/A
pENTR-FLAG-MpMyb14-CO	This study	GenBank: MK835684
pENTR-proMpPR6a	This study	GenBank: MK835683
Software and Algorithms		
ImageJ (Fiji)	https://imagej.net/Fiji/Downloads	Version: 2.0.0-rc-62/1.51 s
Microsoft Powerpoint	Microsoft	Version 16.16.8
Prism 6.0	Graph-Pad	https://www.graphpad.com/
Rstudio	https://www.rstudio.com/	V1.1.383
Primer3	[73, 74]	http://primer3.ut.ee/
MaxQuant version 1.5.7.4,	[75]	http://www.maxquant.org/
Perseus version 1.5.8.5,	[76]	http://www.maxquant.org/
OrthoFinder	[32]	https://github.com/davidemms/OrthoFinder
R package “pheatmap”	R. Kolde	https://github.com/raivokolde/pheatmap
R packages “alluvial”	Bojanowski and Edward	https://cran.r-project.org/web/packages/alluvial/index.html
FastQC	Babraham Bioinformatics	https://www.bioinformatics.babraham.ac.uk/projects/fastqc/
DESeq2	[77]	https://bioconductor.org/packages/release/bioc/html/DESeq2.html
STAR aligner	[78]	https://github.com/alexdobin/STAR
FeatureCounts	[79]	http://bioinf.wehi.edu.au/featureCounts/

LEAD CONTACT AND MATERIALS AVAILABILITY

Further information and requests for resources and reagents should be directed to and will be fulfilled by the Lead Contact, Sebastian Schornack (sebastian.schornack@slcu.cam.ac.uk).

EXPERIMENTAL MODEL AND SUBJECT DETAILS**Plant Growth Details**

Marchantia polymorpha TAK1 (male) liverworts were cultivated from gemmae under axenic conditions on one-half-strength MS (Murashige and Skoog) media (pH 6.7) supplemented with B5 vitamins under continuous light (70 $\mu\text{E} \cdot \text{m}^{-2} \cdot \text{s}^{-1}$) at 22°C. *Nicotiana benthamiana* plants were grown on soil in glasshouse conditions with a controlled temperature of 22–24°C and long-day photoperiod (16 hours of light).

Pathogen Growth Details

The fluorescently labeled *Phytophthora palmivora* strains ARI-td (accession P3914 [72];), ARI-GFP (this study), and LILI-YKDEL (accession P16830 [31];) used in this study were grown in a Conviron growth cabinet set to 25°C with constant light conditions

that are maintained routinely by passaging zoospores onto V8 juice agar plates supplemented with G418 (100 $\mu\text{g}/\text{mL}$) and carbenicillin (50 $\mu\text{g}/\text{mL}$).

METHOD DETAILS

Pathogen Infection Assays

Pathogen colonization experiments were performed by applying 10 μL droplets of a zoospore suspension inoculum (10^5 zoospores per milliliter) along the dorsal thallus surface of 3-week-old *M. polymorpha* liverworts or onto the abaxial surface of detached *N. benthamiana* leaves collected from 3-week-old plants that were subsequently kept on wetted absorbent paper enclosed in plastic dishes to maintain high humidity.

Phytophthora palmivora Transformation

Transformation of *P. palmivora* ARI (accession P3914) with pTOR-GFP [80] was performed as described in [81]. In brief, approximately 40 μg of pTOR-GFP vector was added to 680 μL of a concentrated suspension of ARI zoospores and 80 μL of 10X Petri's solution (2.5 mM CaCl_2 , 10 mM MgSO_4 , 10 mM KH_2PO_4 , 8 mM KCl). This suspension was electroporated with the following settings: voltage at 500 V, capacitance at 50 F, resistance at 800 ohms, with a time constant around 6-7 ms. The electroporated suspension was combined with 6 mL of clarified liquid V8 media in a 15 mL falcon tube and incubated on a gentle rocking shaker for 6 hours at room temperature. Positive GFP expressing transformants were selected on V8 plates containing G418 (100 $\mu\text{g}/\text{mL}$) and carbenicillin (50 $\mu\text{g}/\text{mL}$) 3-10 days after plating.

Microscopy & Histochemical Staining

Confocal laser scanning microscopy was performed using a Leica TCS SP8 equipped with HyD detectors as described in [26]. A white light laser was used to visualize GFP (excitation 488 nm), mCitrine (excitation 509 nm) and YFP (excitation 515 nm). Epifluorescence microscopy was performed on a dissecting Leica M165 FC stereo-epifluorescence microscope using a DSRed filter for the detection of tdTomato fluorescence. Images were obtained using Leica Application Suite V4.1 acquisition software. Images were collected from at least three independent plants in at least two separate infection sites per plant. All experiments were performed at least three times with similar results. Histochemical GUS staining was performed on ARI-td-infected liverworts by vacuum infiltrating plants with a GUS staining solution consisting of 2 mM X-gluc (5-bromo-4-chloro-3-indolyl-beta-D-glucuronic acid, cyclohexylammonium salt), 0.1% Triton X-100, 10 mM EDTA, 2.5 mM potassium hexacyanoferrate II, and 2.5 mM potassium hexacyanoferrate III in a buffered phosphate solution (3.1 g/L sodium phosphate monobasic monohydrate and 10.9 g/L sodium phosphate dibasic anhydrous in double distilled water, pH 7.4). Plants were incubated in staining solution overnight (12-16 hours) at 37°C and were subsequently de-stained in a solution of 70% ethanol with 20% glycerol added. Cross-sections of GUS-stained liverworts were prepared at a thickness of 200-to-300- μm from 3% agarose-embedded samples using a vibratome. All images were processed using ImageJ or Microsoft Powerpoint. Propidium iodide (PI) staining was performed by incubating excised liverwort thalli in 2 $\mu\text{g ml}^{-1}$ propidium iodide solution (in water) for 15 minutes in the dark. PI fluorescence was visualized by confocal laser scanning microscopy (excitation 543 nm, emission detected at 588-628 nm). For analysis of heavily pigmented sectors, on those areas of *proHSP:MpMyb14* where no light transmittance is observable in the bright field channel was considered.

RNA Isolation, cDNA Synthesis, and qRT-PCR Analysis

Total RNA was extracted from flash-frozen *M. polymorpha* (TAK1) plants that were mock-inoculated (water) or infected with *P. palmivora* (ARI-td) zoospores using the PureLink Plant RNA Reagent following the manufacturer's instructions. All total RNA samples were subsequently treated with Turbo DNA-free DNase reagent (Invitrogen) to degrade residual DNA contamination before further use. cDNA was synthesized with SuperScript II reverse transcriptase (Invitrogen) using 2 μg of total RNA following the manufacturer's instructions. All cDNA samples were diluted 10-fold with nuclease-free water and stored at -20°C . qRT-PCR analyses were carried out in 10 μL reactions using 2.5 μL of diluted cDNA and Roche SYBR mix with the primers listed in Table S1. All qRT-PCR experiments were performed using a program consisting of an initial denaturation at 95°C for 5 minutes followed by 40 cycles of 95°C for 10 s, 60°C for 14 s, and 72°C 14 s on a Roche LightCycler 480 II according to manufacturer's instructions. Primers for qRT-PCR analyses were designed using Primer3 [73, 74] and specificity was validated by analyzing melt curves after each run. This study also used previously published primers for *M. polymorpha* housekeeping genes [82], *P. palmivora* transcript quantification [72], and *M. polymorpha* phenylpropanoid pathway analysis [37] (Table S1). Three technical replicates were analyzed for each of three independent sample replicates at any given time point/treatment. Calculations of expression levels normalized to internal controls and statistical analyses (ANOVA, Tukey's HSD) were performed using R software. Graphs were generated in GraphPad Prism6.

Proteomics

Sample preparation

50 mg of powdered *M. polymorpha* tissue were added to 250 μL of extraction buffer (8M Urea in 100mM Tris/HCl pH8.5, complemented with Phosphatase Inhibitor Cocktail 3 (Sigma, P0044-5ML) (20 $\mu\text{l}/\text{ml}$) and Phosphatase Inhibitor Cocktail 2 (Sigma, P5726-5ML) (20 $\mu\text{l}/\text{ml}$) and briefly mixed on a Vibrax shaker. Next, all samples were sonicated for 15 min and subsequently mixed

on a Vibrax shaker for 15 min. After determination of the protein concentration using Pierce 660nm Protein Assay, aliquots of 100 μ g total protein per sample were further processed by in-solution digest. Protein mixtures were reduced with dithiothreitol, alkylated with chloroacetamide, and digested first with Lys-C for 4h and subsequently with trypsin overnight. Samples were then submitted to SDB-RPS fractionation using a protocol adapted from [83]. In brief, stage tips were prepared with 2 layers of SDB-RPS membrane and activated with 100 μ L acetonitrile, followed by equilibration with 100 μ L equilibration buffer (30% (v/v) MeOH, 1% (v/v) TFA) and 100 μ L 0.2% TFA. Peptides were immobilized on the membrane, washed with 100 μ L 0.2% TFA, eluted into 3 consecutive fractions using SDB-RPS buffer 1 (100 mM NH_4HCO_2 , 40% (v/v) ACN, 0.5% FA), SDB-RPS buffer 2 (150 mM NH_4HCO_2 , 60% (v/v) ACN, 0.5% FA) and finally SDB-RPS buffer 3 (5% Ammonia (v/v), 80% (v/v) ACN). The collected fractions were evaporated to dryness to remove residual ammonia.

LC-MS/MS data acquisition

dried peptides were re-dissolved in 2% ACN, 0.1% TFA for analysis and adjusted to a final concentration of 0.1 μ g/ μ L. Samples were analyzed using an EASY-nLC 1200 (Thermo Fisher) coupled to a Q Exactive Plus mass spectrometer (Thermo Fisher). Peptides were separated on 16 cm frit-less silica emitters (New Objective, 0.75 μ m inner diameter), packed in-house with reversed-phase ReproSil-Pur C18 AQ 1.9 μ m resin. Peptides (0.5 μ g) were loaded on the column and eluted for 115 min using a segmented linear gradient of 5% to 95% solvent B (0 min: 5%B; 0-5 min - > 5%B; 5-65 min - > 20%B; 65-90 min - > 35%B; 90-100 min - > 55%; 100-105 min - > 95%, 105-115 min - > 95%) (solvent A 0% ACN, 0.1% FA; solvent B 80% ACN, 0.1%FA) at a flow rate of 300 nL/min. Mass spectra were acquired in data-dependent acquisition mode with a TOP15 method. MS spectra were acquired in the Orbitrap analyzer with a mass range of 300–1750 m/z at a resolution of 70,000 FWHM and a target value of 3×10^6 ions. Precursors were selected with an isolation window of 1.3 m/z. HCD fragmentation was performed at a normalized collision energy of 25. MS/MS spectra were acquired with a target value of 105 ions at a resolution of 17,500 FWHM, a maximum injection time of 55 ms and a fixed first mass of m/z 100. Peptides with a charge of +1, greater than 6, or with unassigned charge state were excluded from fragmentation for MS2, dynamic exclusion for 30 s prevented repeated selection of precursors.

Data analysis

Raw data were processed using MaxQuant software (version 1.5.7.4, <http://www.maxquant.org/>) [75] with label-free quantification (LFQ) and iBAQ enabled [76]. MS/MS spectra were searched by the Andromeda search engine against a combined database containing the sequences from *M. polymorpha* (primary transcripts; http://marchantia.info/download/download/Mpolymorphav3.1.primaryTrs.pep_annot.fa.gz), *Phytophthora palmivora* [71] and sequences of 248 common contaminant proteins and decoy sequences. Trypsin specificity was required and a maximum of two missed cleavages allowed. Minimal peptide length was set to seven amino acids. Carbamidomethylation of cysteine residues was set as fixed, oxidation of methionine and protein N-terminal acetylation as variable modifications. Peptide-spectrum-matches and proteins were retained if they were below a false discovery rate of 1%. Statistical analysis of the MaxLFQ values was carried out using Perseus (version 1.5.8.5, <http://www.maxquant.org/>). Quantified proteins were filtered for reverse hits and hits “identified by site” and MaxLFQ values were log2 transformed. After grouping samples by condition (4 groups) only those proteins were retained for the subsequent analysis that had two valid values in one of the conditions. Missing values were imputed from a normal distribution, using the default settings in Perseus (1.8 downshift, separately for each column). Volcano plots were generated in Perseus using an FDR of 0.01 and an $s_0 = 1$, data was exported and processed using Excel. For comparisons against RNA-seq data, we considered significantly differentially abundant protein loci (LFC > 1) with 1 unique peptide fragment identified in the fractionated analyses that mapped to the *Marchantia polymorpha* proteome. The accession number for proteomics data generated in this study is PRIDE: PXD012076.

Cloning and Marchantia Transformation

Promoter regions of MpPR6a (Mapoly0448s0001) and MpPRX/PR9 (Mapoly0106s0049; described in [26] and the coding region of MpMyb14 (Mapoly0073s0038) were synthesized with flanking attL sites by Genewiz for direct recombination into *Marchantia* Gateway destination vectors [39]. The accession numbers for synthesized sequences are GenBank: MK835684, MK835683. The *pro*MpPR6a/MpPRX:tdTomato-NLS and *pro*MpPR6a:GUS constructs were generated by recombination into pMpGWB316 and pMpGWB104 using LR clonase II enzyme mix (Invitrogen) according to the manufacturer’s directions. MpMyb14 expression vectors were similarly generated by LR recombination into pMpGWB105 (*pro*35S:mCitrine-flag-MpMyb14) and pMpGW132 (*pro*HSP:flag-MpMyb14). The resulting constructs were transformed into *Agrobacterium tumefaciens* GV3101 (pMP90) by electroporation. *M. polymorpha* transformation was carried out using the *Agrobacterium*-mediated thallus regeneration method using TAK1 plants [84]. Transformants were selected on solidified 1/2 MS media (pH 5.6) supplemented with cefotaxime (125 μ g/mL) and hygromycin B (15 to 25 μ g/mL) or chlorsulfuron (0.5-1 μ M). Stable, non-chimeric transgenic plants were obtained by propagating gemmae from T1 thalli.

Library preparation and sequencing

mRNAs from *M. polymorpha* plants infected with *P. palmivora* ARI-td at 1, 2, 3 and 4 dpi, and *N. benthamiana* leaves infected with *P. palmivora* ARI-td at 14, 24, 48 and 72 hpi and respective mock-inoculated control samples were purified using Poly(A) selection from total RNA sample, and then fragmented (at least 2 independently infected plants collected per sample replicate). cDNA library preparation was performed with the TruSeq RNA Sample Preparation Kit (Illumina, US) according to the manufacturer’s protocol. cDNA sequencing of each sample (all in triplicates) was performed with Illumina HiSeq 2500 in 100 (*Marchantia*) or 150 (*Nicotiana*)

paired end mode. Samples were de-multiplexed and analyzed further. The raw fastq data are accessible at <http://www.ncbi.nlm.nih.gov/sra/> with accession numbers NCBI SRA: PRJNA397637 (*Marchantia-Phytophthora*) and NCBI SRA: PRJNA503573 (*Nicotiana-Phytophthora*).

Expression analysis

Raw reads first analyzed with FastQC for quality control (<https://www.bioinformatics.babraham.ac.uk/projects/fastqc/>) were aligned back to the respective plant genome (*Marchantia polymorpha* v3.1 and *Nicotiana benthamiana* draft genome sequence v1.0.1) using STAR (version 2.5.2b) aligner [78]. Raw counts were obtained with featureCounts [79] and only uniquely mapped and properly paired reads were considered further. Differentially expressed genes were identified with DESeq2 Bioconductor package [77] following pairwise comparisons between infected and mock-inoculated samples at the same stage of infection. Differentially expressed genes (absolute LFC [\log_2 fold change] ≥ 2 and adjusted p value $\leq 10^{-3}$) were used to perform hierarchical clustering of samples. Heatmaps for the differentially expressed genes were generated using R pheatmap package using variance-stabilized counts median-centered by gene. Scripts used to analyze RNA-seq datasets and visualize differentially expressed genes are available at <https://github.com/gogleva/Marchantia>. Summary *M. polymorpha* functional gene annotations were created based on [15]. Tidy summary annotations are also available at <https://github.com/gogleva/Marchantia>. Alluvial diagrams displaying the dynamics of annotated *M. polymorpha* genes differentially expressed during *P. palmivora* infection were performed in R using the ‘alluvial’ package.

Orthology analysis

To reconstruct orthogroups between *M. polymorpha* and *N. benthamiana*, we used OrthoFinder (OrthoFinder-2.2.7 [32]) with respective plant proteomes. For this analysis only primary protein isoforms were used. Output files were parsed and further analyzed in R (scripts and raw outputs are available at <https://github.com/gogleva/Marchantia>). Following differential expression analysis (only genes with adjusted p value $< 10^{-3}$ were considered), we used LFC of single-copy orthologs to assess similarity of *M. polymorpha* and *N. benthamiana* responses to infection with *P. palmivora* (strain ARI-tdTomato). Based on previous characterization of *Phytophthora* infection dynamics [26, 31], we considered infection stages to be comparable between *M. polymorpha* and *N. benthamiana* infection time courses in the following layout: 1 dpi - 14 hpi; 2 dpi - 24 hpi; 3 dpi - 48 hpi; 4 dpi - 72 hpi).

QUANTIFICATION AND STATISTICAL ANALYSIS

Statistical details of experiments can be found in the corresponding figure legends. Here, the identity of the statistical tests used, the exact value of n (i.e., number of independently infected liverworts) and dispersion and precision measures are given (error bars represent mean \pm standard deviation, p value cutoffs, etc.). All statistical analyses for transcriptomic and proteomic analyses are described in the [Method Details](#) above. Statistical analysis of qRT-PCR expression data are described in figure legends and were performed using R.